CRUISE REPORT

R/V Melville
May 4 - 18, 2012
Valparaiso, Chile - Valparaiso, Chile

The 2010 Maule, Chile Earthquake:
Project Evaluating Prism Post-Earthquake Response
(Chile-PEPPER)

Chief Scientist - Anne Tréhu, Oregon State University
Co-Chief Scientist - Mike Tryon, Scripps Institution of Oceanography

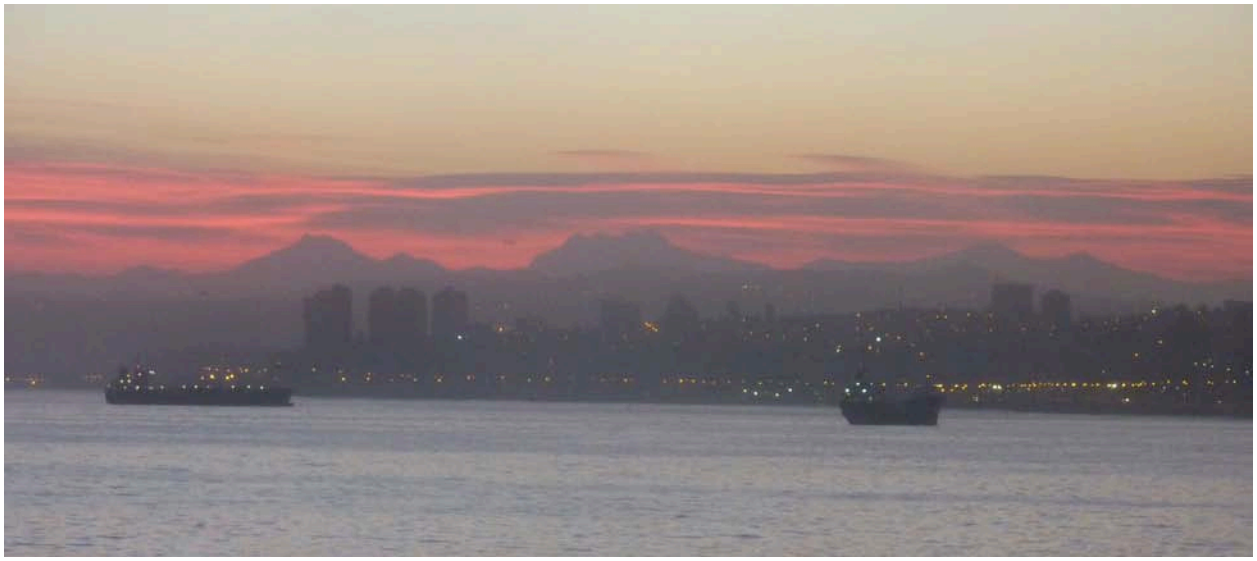

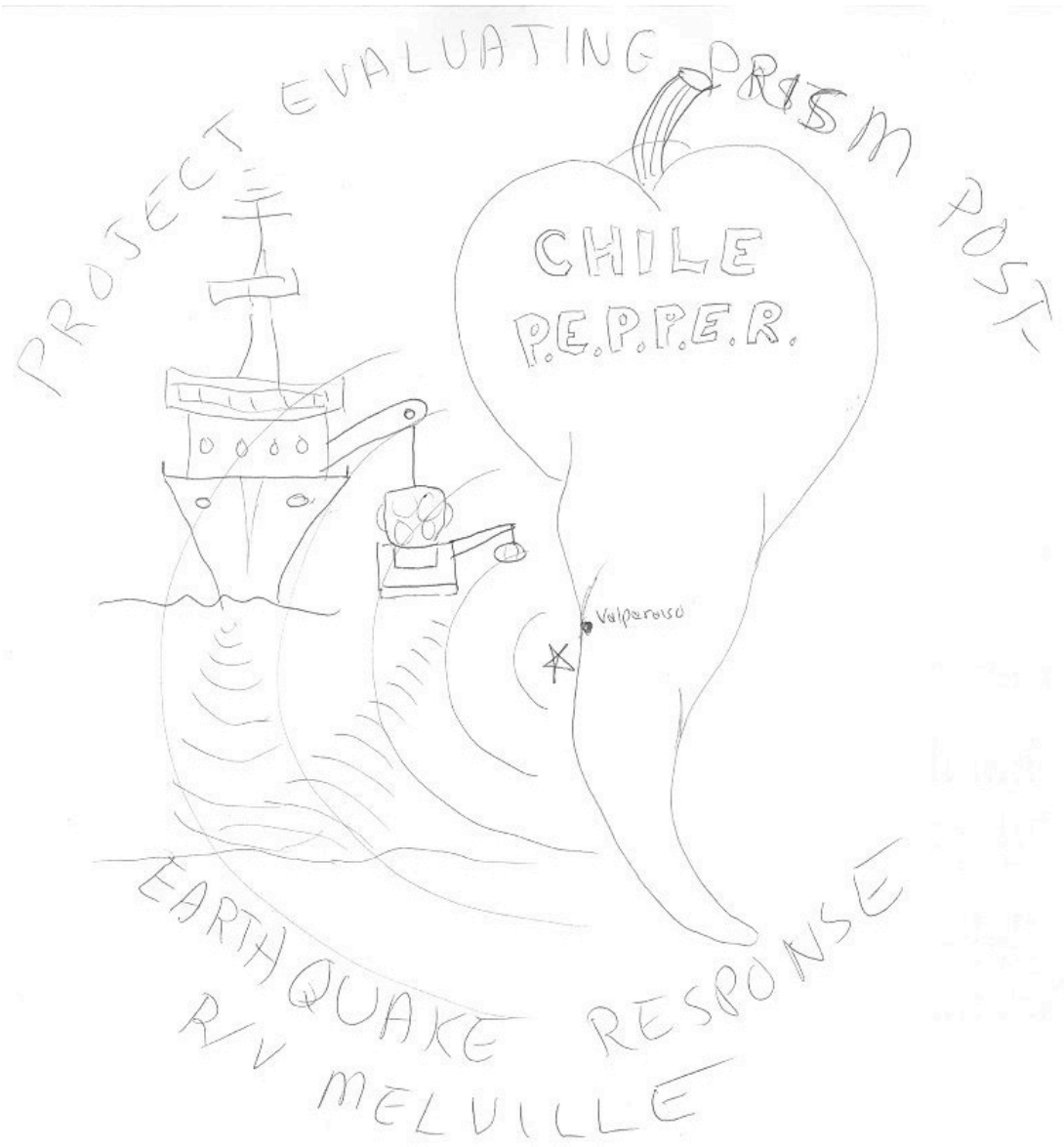
PROJECT EVALUATING PRISM POST
CHILE
P.E.P.P.E.R.
Valparaiso
EARTHQUAKE RESPONSE
R/V MELVILLE

TABLE OF CONTENTS

note: All data from this cruise are publically available, or will be available after a 2-year proprietary period. The group to contact for data is indicated in the corresponding chapter in the report.

Science Party:

Oregon State University
Chris Kenyon, student
Yi Lou, visiting student
Mark Williams, student

Universidad de Chile Santiago:
Emilio Vera Sommer, professor
Eduoardo Contreras Reyes, professor
Emilio Bravo, student
Natalia Cornejo, student
Felipe Gonzalez, student
Andrei Maksymowicz, student

Scripps Institution of Oceanography
Lee Ellett, seismic technician
Jon Meyer, computer technician
Keith Shadle, technician
Jay Turnbull, seismic technician

Lamont Doherty Earth Observatory
David Gassier, engineer
Ted Koczynski, engineer
Vincent Oletu, technician
Drew Stolzman, technician

Marine Mammal Observers
Chris Cutler
Patti Haase
Paula Olson

Chilean Observer
Patricio Opaza Arriagada

Crew:

Murline, David, Master
Lawrence, Ian, 1st Officer
Kirby, Jeff, 2nd Officer
Chae, Eugene, 3rd Officer
Grimes, David, Bosun
Ball, Rob, Able Seaman
Shute, Paul, Able Seaman
Vinkovits, Sandor, Able Seaman
Martino, Joseph, OS
Smith, Mark, Cook
Seeley Robert, Cook
Rodriquez, Alex, Ch. Engineer
Fitzgerald, Patrick, 1st Asst. Eng.
Clevelan, Danniel, 2nd Asst. Eng.
Coogen, Cory, 3rd Asst. Eng.
Weinke, Antje, Electrician
Brown, William, Oiler
Juhasz, Robert, Oiler
Bautista, Eduardo, Oiler
Hogan, Philip, Oiler
Porcioncula, Tony, Wiper

MV1206 Science Party

Overview of Scientific Objectives and Data Acquired

Based on seismological, geodetic and bathymetric data, it appears that the February 27, 2010 M8.8 subduction zone earthquake beneath central Chile did not rupture to the seafloor during the earthquake (Fig. 1). This contrasts with the March 11, 2011 Tohoku earthquake offshore northeast Japan, which clearly did rupture to the seafloor, resulting in a devastating tsunami. Although the 2010 earthquake generated considerable damage both through ground shaking and because of locally high tsunami run-ups, tsunami damage was not as great as it would have been if the earthquake had ruptured to the seafloor.

Expedition MV1206 of the R/V Melville was designed to study how the outer sedimentary accretionary wedge is adjusting to the change in stress caused by slip that occurred at greater depth on the plate boundary during the 2010 earthquake. Several different kinds of data were (or are currently being) acquired. The primary objective of the cruise was to deploy 10 broadband ocean bottom seismometers (BB-OBS) with integrated flow meters updip from the patch of greatest slip during the 2010 earthquake (Fig. 1, 2). These instruments will be recovered in March 2013. This cruise represents the first time chemical and aqueous transport (CAT) flow meters have been integrated with the ocean bottom seismometers (OBS) from the NSF-sponsored ocean bottom seismology instrument pool (OBSIP) at the Lamont-Doherty Earth Observatory (LDEO). Motivation for this effort was provided by the recognition that the hydrogeologic system is directly coupled to the tectonic system through the interaction of fluid pressure and stress state. Temporal records of pore pressure changes have been demonstrated to correlate with regional tectonic stresses and seismic activity in a number of places, e.g. the Juan de Fuca Ridge [*Davis et al.*, 2001], Nankai [*Davis et al.*, 2006], Costa Rica [*Davis and Villinger*, 2006], and Caucasian orogenic wedge [*Kopf et al.*, 2005]. In the aftermath of a major subduction-thrust earthquake, the distribution of stress and pore fluid pressure is strongly altered in the region of the wedge updip of the rupture. During the subsequent recovery stage, fluid flow should result from this newly imposed pressure distribution, further altering the pressure distribution and effective stress state throughout the updip region. Due to the high hydraulic impedence of typical seafloor sediments, this redistribution should take place over many years and will tend to be focused on preexisting zones of fracture permeability such as out-of-sequence thrusts (OOST). This should lead to slip on faults and other zones of weakness resulting in a heterogeneous pattern of microsesimicity, tremor, and aseismic deformation. Half of the BB-OBSs are also equipped with absolute pressure gauges (APG) to detect possible seafloor uplift. The others have differential pressure gauges.

In addition to the OBS deployment, we acquired a variety of other datasets, including ~1500 km of new high-resolution multi-channel seismic reflection data (Fig. 2). The seismic source was two GI-guns shot simultaneously in 45/105 configuration. The shots were recorded on a 48-channel, 600-m-long streamer, which became a 40-channel, 400-m-long streamer after a shark attack resulted in the loss of 2 out of 8 sections; unfortunately only one fully-functional spare section was available. Gravity, acoustic doppler current profiling (ADCP), 3.5 kHz sub-bottom profiling and swath bathymetric (EM-122) data were acquired along all tracks, and magnetic data were acquired along selected tracks. Eighteen expendible bathythermographs (XBT) were

acquired to correct for the acoustic velocity in the water column and provide constraints for interpreting possible reflectivity from within the ocean.

By comparing our new data to data being obtained by others offshore NE Japan, we hope to develop new insights into why slip during some subduction zone megathrust earthquakes extends to the seafloor and why it is arrested at shallow depth in other events. This knowledge could lead to more precise forecasts of where large tsunamis are likely to be generated around the globe.

An important aspect of MV1206 was education. The seven students on board processed seismic, magnetic and bathymetric data on board as well as standing watch, and shipboard discussions included informal lectures about the principles underlying the procedures. There were also several opportunities for community outreach. One example - a local newspaper article about the project prior to the cruise - is included as Appendix 1. At the end of the cruise, we participated in two tours of the ship by local high school and university students and in an interview for a local television station.

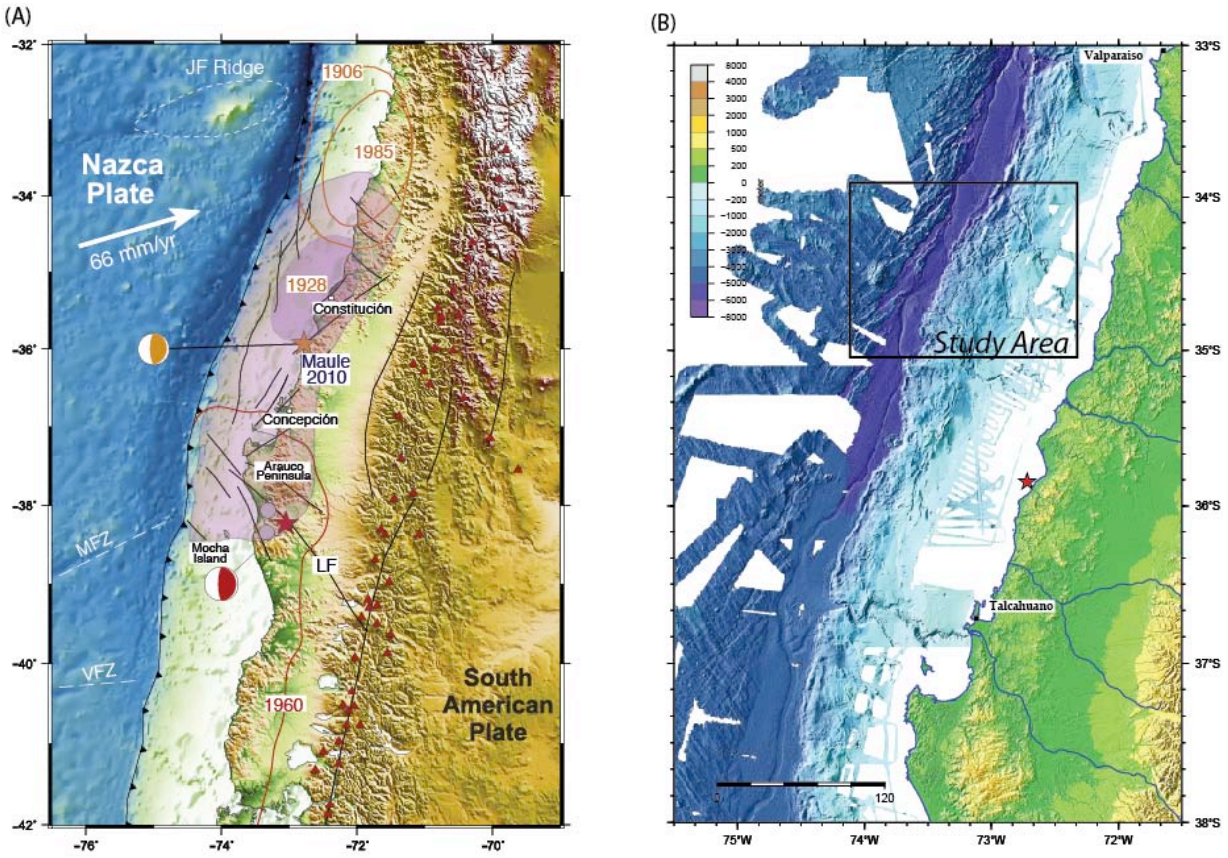

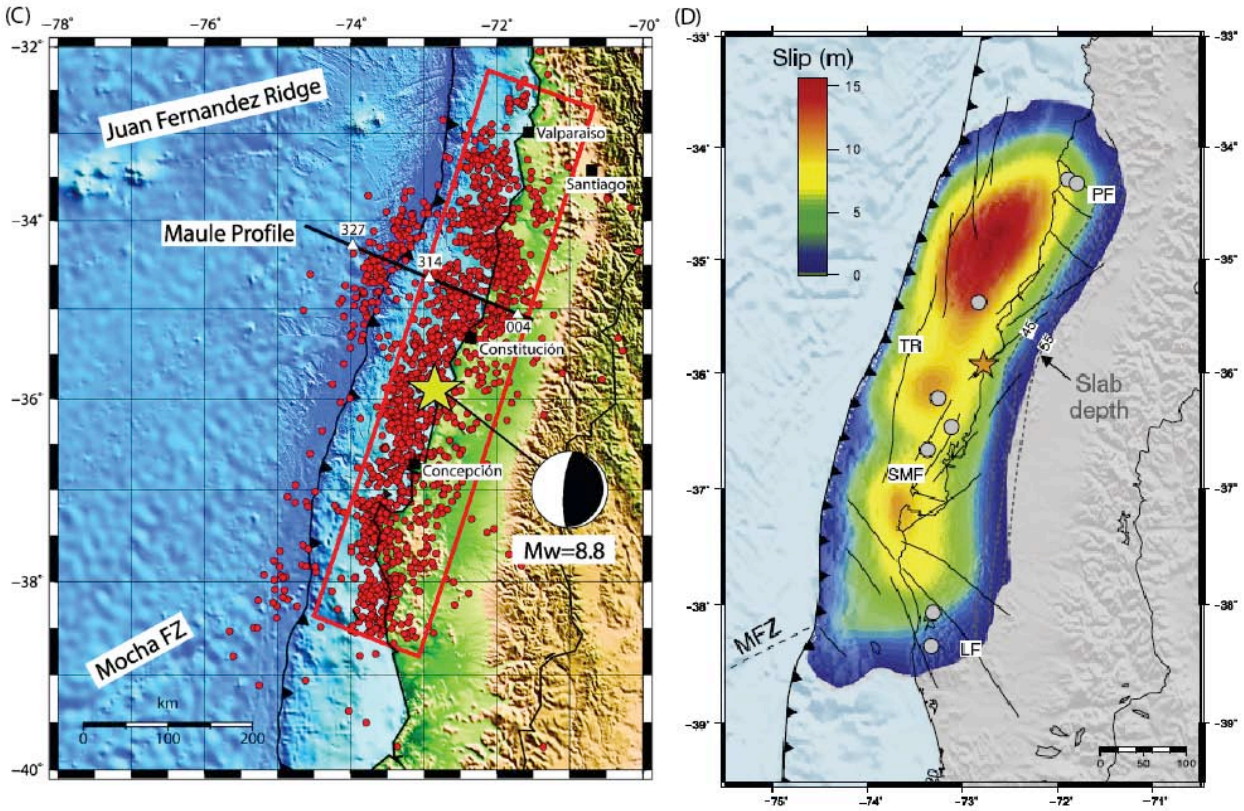

Figure 1. (A) Map of central Chile showing locations of historic earthquakes. The pink shaded area shows the rupture plane of the M8.8 2010 Maule earthquake; the yellow star and "beach-ball" show the epicenter and fault mechanism, respectively. The darker pink region shows the rupture plane of the M8.0 Talca earthquake of 1928. The patch of greatest slip in 2010 (see 1D) is approximately coincident with the patch that slipped during the 1928 event. The red line shows the rupture plane of the M9.5 1960 Valdivia earthquake, with the red star and "beach-ball" showing the epicenter and mechanism. Rupture planes of events in 1906 and 1985 are also outlined. Triangles are volcanoes. (adapted from Moreno et al., 2012). (B) Bathymetric map of the region showing the location of the study area as shown in Figure 2. Data from various GEOMAR cruises conducted prior to 2010. (C) Aftershocks of the 2010 earthquake (Moscoso et al., 2011). Note intense aftershock activity in the subducting plate at the latitude of the study area and the relative lack of aftershocks in the accretionary prism. (D) Slip model from Moreno et al. (2012). While slip models from various investigators differ somewhat, depending on which data or analysis approaches were used, all models show the greatest slip near 35°S.

(A)

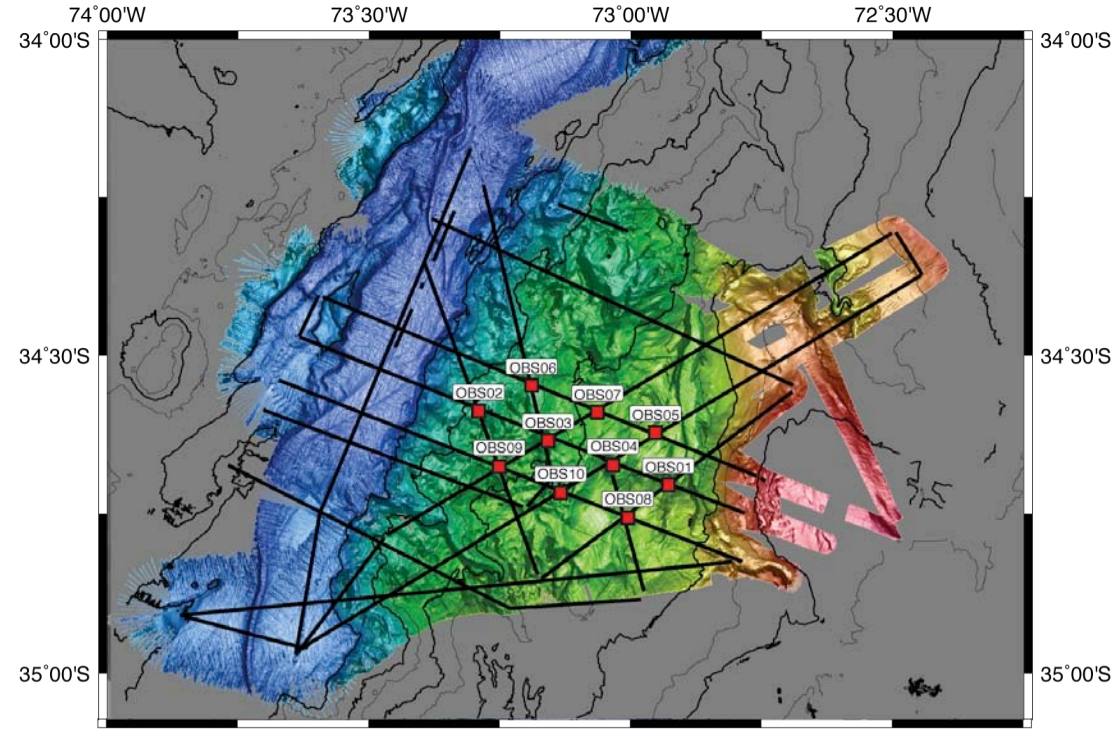

(B)

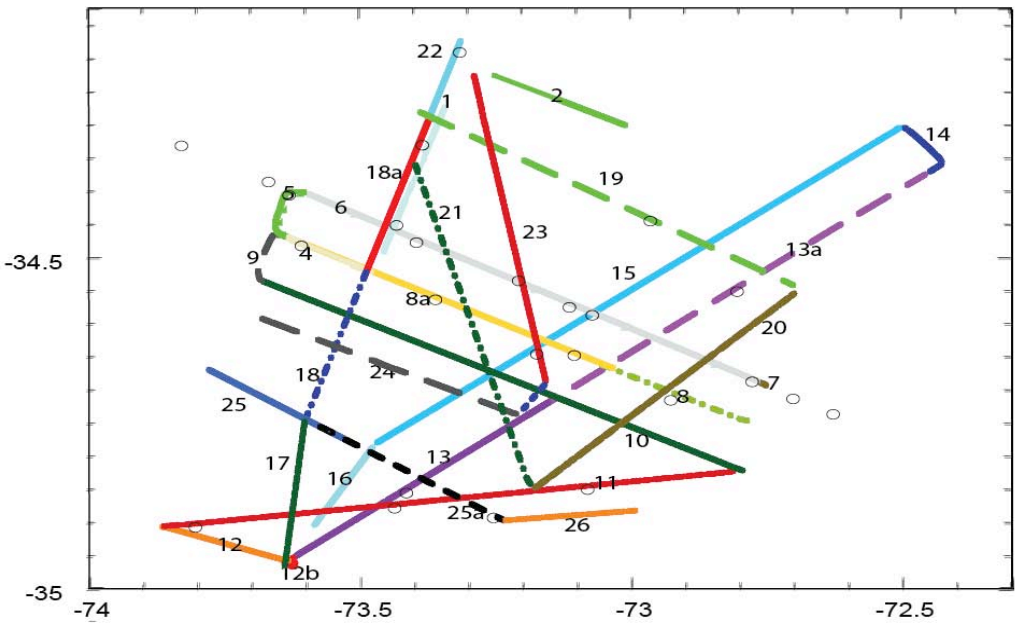

Figure 2. (A) Map showing preliminary bathymetric grid constructed from new data acquired during this cruise and locations of OBSs and seismic reflection lines. (B) Map showing numbering of seismic lines and locations of XBTs (circles).

Tectonic Setting

The southern central Chilean margin (32°-46°S) is characterized by the subduction of the oceanic Nazca plate beneath South America at a present rate of ~66 km/Myr [*Angermann et al*., 1999] in a N78°E direction, although the rate averaged over several million years is ~85 km/Myr [*DeMets et al*., 1994]. The Juan Fernandez Ridge (JFR) enters the trench at ~33°S and acts as a barrier to northward transport of trench turbidites, resulting in a sediment-starved trench to the north and a sediment-flooded trench to the south [*von Huene et al*., 1997] (Fig. 3). The high sedimentation rate in the trench between the JFR and the Chile Triple Junction (CTJ) is the result of high sedimentation rates since the Pliocene linked to glaciation/deglaciation and fast denudation of the Andes [e.g., *Melnick and Echtler*, 2006; *Kukowski and Oncken*, 2006]. The deposited material is mainly transported through deep canyons and redistributed within the trench from south to north [*Thornburg et al*., 1990; *Voelker et al*., 2011]. The submarine canyons are offshore prolongations of the main rivers of Pleistocene glacial valleys and cut across the continental shelf and slope [*Gonzalez*, 1989]. Three of these canyons cut through the study area.

The seawardmost part of the south central Chile forearc (33°-46°S) comprises a 5-50 km wide frontal accretionary prism, which abuts the truncated continental basement (inner prism) that extends seaward from beneath the shelf [*Contreras-Reyes et al*., 2010]. The relatively small amount of sediment in the prism is not compatible with a continuous history of accretion, which implies episodic phases of tectonic accretion, nonaccretion, and erosion [*Bangs and Cande*, 1997]. *Melnick and Echtler* [2006] and *Kukowski and Oncken* [2006] have argued that the accretionary prism started to form as a response to a rapid increase of glacial age sediment supply to the trench during the middle Pliocene. *Contreras-Reyes et al*., [2010] characterized the southern central Chile margin by two main segments that present differences in their frontal accretionary prism (FAP) size and subduction channel thickness. The northern Maule segment is characterized by a FAP 20-50 km wide and a subduction channel typically thinner than 1 km [*Moscoso et al*., 2011]. The southern Chiloé segment is characterized by a small FAP (<10 km wide) and a thick subduction channel (~1.5 km) [*Schewarth et al.*, 2009]. Our study, which shows that the along-strike transition from sediment accretion to sediment subduction can be very abrupt, occurring over a few km, with little overall change in the width of the prism, however, suggests that the character of the deformation front changes with time as well as along strike. The factors controlling whether sediment is accreted or subducted are probably complex and not immediately evident.

Seismic data were acquired along the Maule segment by the Chilean vessel Vidal Gormaz in 2002/2003 [*Contardo et al*., 2008] and by the British vessel James Cook in 2008 [*Flueh and Bialas*, 2008; *Moscoso et al*., 2011]. *Contardo et al*., [2008] discussed faulting along the continental slope in the Maule segment, where the continental shelf is 30-40 km wide and the forearc sedimentary basin is 1,500-2,000 m thick. *Moscoso et al*., [2011] presented a detailed 2D seismic velocity model from a 2D active-source profile located across the margin in the epicentral region of the megathrust earthquake of 2010. These authors found a frontal accretionary prism 40-50 km wide whose landward limit spatially correlates with the continental shelf break, which is characterized by a prominent ~2 km fault scarp that extends more than 300 km along strike [*Contardo et al*., 2008; *Voelker et al*., 2011].

Figure 3A. Geodynamic setting of Nazca, Antarctic, and South America plates. These three plates come together at the Chile triple junction (CTJ). The south-central Chile margin is heavily sedimented and lies between the Juan Fernández Ridge (JFR) and Chile Rise spreading center. The Chile trench and Mocha and Valdivia fracture zones define the Mocha block (MB), which separates young (0– 25 Ma) oceanic lithosphere to the south from old (30– 35 Ma) lithosphere to the north [Tebbens et al., 1997]. B. Depth of the trench axis along the Chilean trench and trench fill thicknesses after Contreras-Reyes and Osses, [2010].

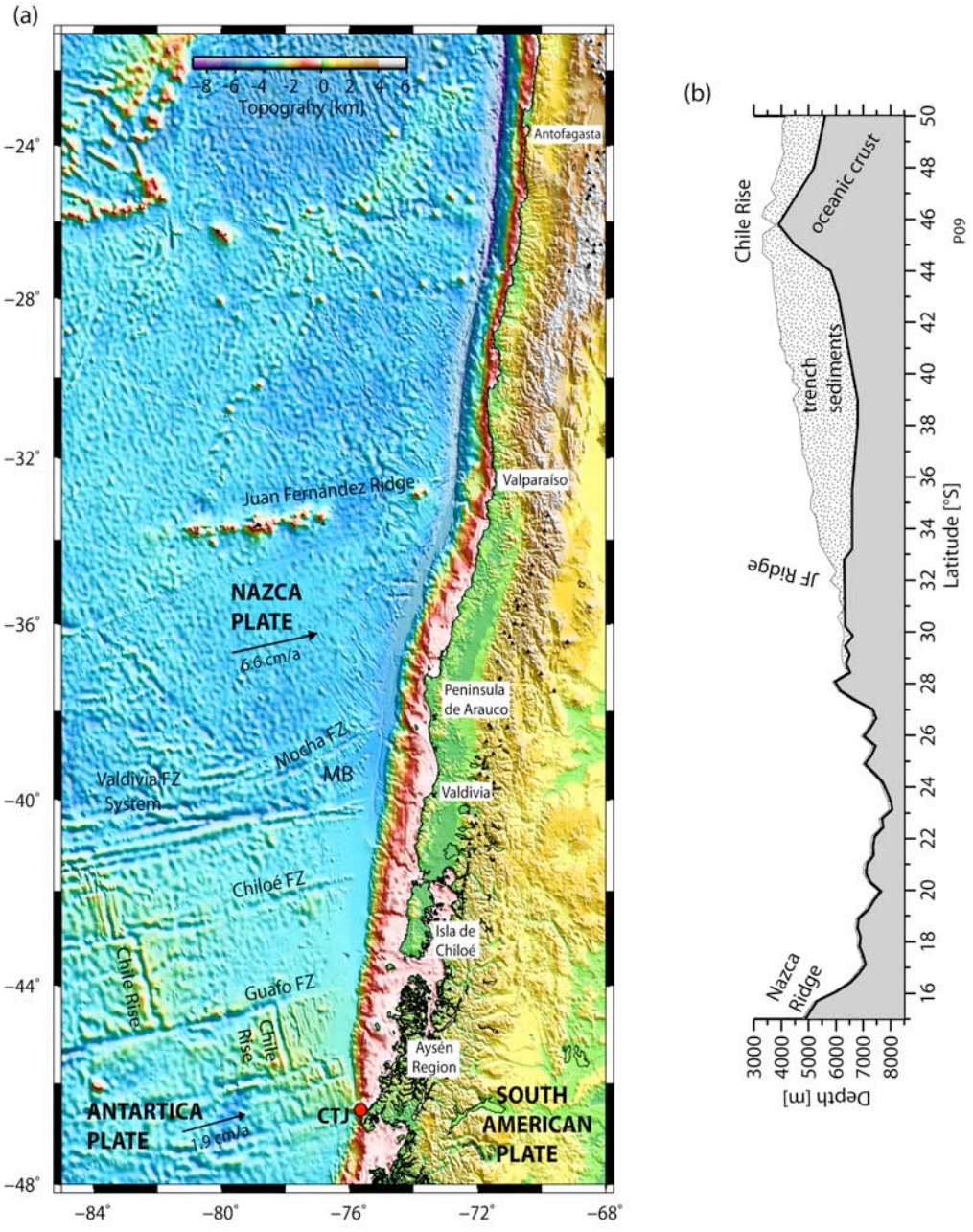

Ocean bottom seismometers

Broadband ocean bottom seismometers (BB-OBS) were provided by the Ocean Bottom Seismograph Instrument Pool (OBSIP), supported by the National Science Foundation. The OBSIP comprises 3 pools of instruments operated by the Lamont-Doherty Earth Observatory (LDEO), the Scripps Institution of Oceanography (SIO) and the Woods Hole Oceanographic Institution (WHOI). Scientists request instruments from the pool as part of the proposal process and are assigned instruments from one of the facilities according to instrument availability. This experiment was supported by the LDEO group, which provided 10 broadband (BB) OBSs. Five were the LDEO standard BB OBS, equipped with a 3-component L4C 1 Hz geophone with a low-noise amplifier, which nominally provides useful signal down to 100 s period, and a differential pressure gaug,e and five were the new LDEO 2001 model seismometer, equipped with a Trillium Compact seismometer, Paroscientific absolute pressure gauge, and a hydrophone, which was developed with support from the American Recovery and Reinvestment Act of 2009 (ARRA). Both types of seismometers are recording 100 samples/second. Photographs of the instruments and more details about their technical specifications are found in Appendix 2.

The two instuments have somewhat different capabilities (Appendix 2). Both contain seismic sensors in a separate package, which is deployed along side the main recording and battery package by a retractable arm. In addition, all 10 OBSs were modified for this cruise to incorporate CAT fluid flow meters into the main recording package (see section 4).

Instrument deployment sites were chosen to provide good resolution for microearthquakes and other possible seismic events (e.g. tremor, slow earthquakes) occurring in the accretionary prism seaward of the forearc basement crust as defined by previous seismic refraction experiments. There is a trade-off between the size of the region that could be covered and instrument spacing. To attain good depth resolution, we decided on an inter-OBS spacing <10 km, which allowed us to cover of a segment of the lower continental slope with relatively smooth topography located between 2 submarine canyons. Alternative deployment patterns were considered that would extend to the abyssal plain, but would have either greater inter-instrument spacing or less along-strike coverage and were rejected in favor of the pattern shown in Figure 2.

Instruments were relocated on the seafloor by acoustically ranging to them in a circular pattern with a diameter approximately equal to the water depth. Appendix 3 shows the ranging pattern and uncertainty of the solutions for each instrument. In all cases, the OBSs settled within 215 m of the original target site. Planned and actual OBS locations are given in Table 1. OBSs will be recovered in Spring 2013, and a brief addendum to this report will be prepared at that time.

Table 1. *OBS information.* ***A.*** *Identification codes for various instrument components.* ***B.*** *Final instrument positions on the seafloor determined through inversion of travel times observed during an acoutic survey.* ***C.*** *Originally planned locations. Locations may have been modified somewhat based on bathymetric data collected during the cruise.* ***D.*** *Location where the OBS was dropped and the calculated distance and azimuth between the drop position and the final position on the seafloor.*

Instrument information

site #	frame #	CAT #	OBS type	radio freq	sensor #	DPG SN#	APG #	logger	ampling H	deploy time	on bottom time
1	C12	2	Cascadia	154.585	653		121754	TREHU3	125	129:18:01	5/9/12 18:49
2	C14	4	Cascadia	160.785	723		121760	TREHU5	125	130:18:17	5/10/12 19:41
3	C13	3	Cascadia	160.785	693		121757	TREHU2	125	130:14:03	5/10/12 15:16
4	C15	5	Cascadia	160.725	701		121758	TREHU4	125	129:21:23	5/9/12 22:20
5	A02	9	standard	159.480	2349	37		ICHIRO	40	126:16:33	5/6/12 17:24
6	A22	6	standard	160.785	3299	46		12-ERIN	40	126:10:28	5/6/12 11:50
7	A21	0	standard	159.480	1696	36		26-HOMER	40	126:13:44	5/6/12 14:42
8	A09	8	standard	160.785	2863	69		17-HERO	40	126:22:56	5/6/12 23:46
9	A07	7	standard	159.480	2802	14		KYLIE	40	126:19:46	5/6/12 20:54
10	C11	1	Cascadia	154.585	710		121759	TREHU1	125	130:02:01	5/10/12 3:15

Surveyed locations

site #	frame #	CAT #	lat	deg	min	lon	deg	min	easting	northing	depth
1	C12	2	34.70182	34	42.1091	72.93232	72	55.9394	689376	6158077	2395
2	C14	4	34.58622	34	35.1734	73.29314	73	17.5884	656542	6171518	3924
3	C13	3	34.63270	34	37.9617	73.16094	73	9.6565	668574	6166150	3272
4	C15	5	34.67109	34	40.2652	73.03790	73	2.2739	679771	6161679	2673
5	A02	9	34.61964	34	37.1786	72.95682	72	57.4089	687316	6167238	2550
6	A22	6	34.54564	34	32.7382	73.19254	73	11.5524	665850	6175858	3623
7	A21	0	34.58792	34	35.2754	73.06748	73	4.0486	677237	6170956	2790
8	A09	8	34.75379	34	45.2271	73.00970	73	0.5817	682173	6152456	2398
9	A07	7	34.67334	34	40.4004	73.25416	73	15.2494	659950	6161795	3224
10	C11	1	34.71460	34	42.8759	73.13726	73	8.2356	670577	6157027	2967

Originally planned locations

site #	frame #	CAT #	lat	deg	min	lon	deg	min	easting	northing	depth
1	C12	2	34.70183	34	42.1098	72.93169	73	55.9014	689433	6158078	2397
2	C14	4	34.58588	34	35.1528	73.29272	73	17.5632	656583	6171553	3920
3	C13	3	34.63175	34	37.9050	73.16003	73	9.6018	668662	6166248	3290
4	C15	5	34.67251	34	40.3506	73.03813	73	2.2878	679749	6161523	2667
5	A02	9	34.61969	34	37.1814	72.95638	72	57.3828	687355	6167231	2556
6	A22	6	34.54436	34	32.6616	73.19103	73	11.4618	665994	6175993	3625
7	A21	0	34.58672	34	35.2032	73.06633	73	3.9798	677348	6171090	2776
8	A09	8	34.75273	34	45.1638	73.00884	73	0.5304	682258	6152575	2412
9	A07	7	34.67378	34	40.4268	73.25415	73	15.2490	659946	6161744	3235
10	C11	1	34.71452	34	42.8712	73.13688	73	8.2128	670610	6157037	2975

Drop locations **Drift during descent**

site #	frame #	CAT #	lat	deg	min	lon	deg	min	easting	northing	depth	dist (m)	direction (°)
1	C12	2	34.70150	34	42.0900	72.93000	72	55.8000	689589	6158108	2395	215	262
2	C14	4	34.58589	34	35.1531	73.29224	73	17.5344	656629	6171552	3924	93	249
3	C13	3	34.63163	34	37.8978	73.15978	73	9.5868	668681	6166270	3273	161	222
4	C15	5	34.67183	34	40.3100	73.03667	73	2.2000	679879	6161598	2673	135	307
5	A02	9	34.61983	34	37.1900	72.95550	72	57.3300	687437	6167218	2550	123	279
6	A22	6	34.54447	34	32.6680	73.19109	73	11.4653	665985	6175982	3623	183	227
7	A21	0	34.58654	34	35.1922	73.06607	73	3.9640	677367	6171111	2776	202	220
8	A09	8	34.75285	34	45.1708	73.00916	73	0.5494	682221	6152565	2398	119	204
9	A07	7	34.67400	34	40.4400	73.25450	73	15.2700	659918	6161722	3224	80	24
10	C11	1	34.71437	34	42.8624	73.13660	73	8.1961	670638	6157048	2967	65	251

Chemical and Aqueous Transport (CAT) Meters

The Chemical and Aqueous Transport (CAT) meter [*Tryon et al.*, 2001] is designed to quantify both inflow and outflow rates on the order of 0.01 cm/yr to 100 m/yr. At high outflow rates, a time series record of the outflow fluid chemistry may also be obtained. These instruments have been in use since 1998 and have been very successful in monitoring long term fluid flow in both seep and non-seep environments. The CAT meter uses the dilution of a chemical tracer to measure flow through the outlet tubing exiting the top of a collection chamber. The pump contains two osmotic membranes that separate the chambers containing pure water from the saline side that is held at saturation levels by an excess of NaCl. Due to the constant gradient, distilled water is drawn from the fresh water chamber through the osmotic membrane into the saline chamber at a rate that is constant for a given temperature. The saline output side of the pump system is rigged to inject the tracer while the distilled input side of the two pumps are connected to separate sample coils into which they draw fluid from either side of the tracer injection point. Each sample coil is initially filled with deionized water. Having two sample coils allows both inflow and outflow to be measured. A unique pattern of chemical tracer distribution is recorded in the sample coils allowing a serial record of the flow rates to be determined. Upon recovery of the instruments the sample coils are subsampled at appropriate intervals and analyzed using a Perkin-Elmer Optima 3700 ICP-OES. Both tracer concentration and major ion concentration (Na, Ca, Mg, S, K, Sr, B, Li) are determined simultaneously. A subset of these instruments are equipped with an auxillary osmotic pump connected to copper coils and high pressure valves so that they can be returned to the surface at ambient pressure, maintaining the gas composition of the fluids for analysis.

As explained in Tryon et al. [2001], diffusion in the sample coils is negligible. Typical sample sizes are 25-75 cm of tubing, many times the characteristic diffusion length for typical seawater ions at ocean bottom temperatures. Past experience with year-long deployments has shown that resolutions of ~0.5% of the deployment time in the most recent portions and ~2% in the oldest portion of the record. Resolution is, of course, somewhat dependent on seep flow rate simply because of faster transit times through the instrument, particularly with regards to the chemical resolution. CAT meter locations are the same as OBS locations (Table 1). Data availability will be summarized once the instruments have been recovered.

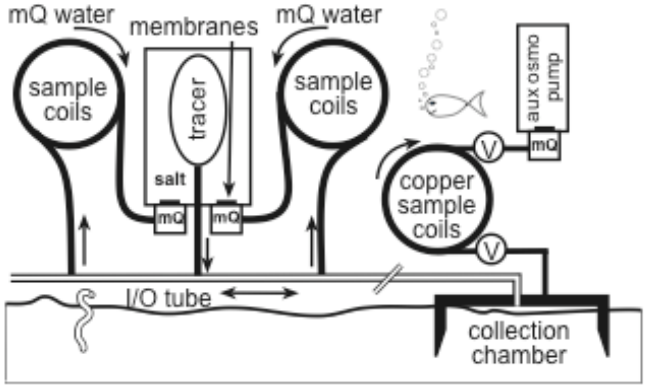

Figure 4. CAT meter schematic [Tryon et al., 2001].

Multichannel Seismic (MCS) data

MCS data were acquired by the SIO Shipboard Geophysical Group (SGG) using a 600-m, 48-channel streamer. The number of channels, however, was decreased to 40 soon after the beginning of the cruise because of shark bites that penetrated two of the 8-channel streamer sections. Fortunately a spare section was available. The source was two GI-guns in a 45/105 cm^3 configuration. The guns were mounted on a cross-bar that maintained them a constant distance apart and were shot at an interval of 25 m as determined from the GPS, with the ship's speed through the water maintained at 4-5 kts. The record length was 9 s for most of the survey, but was increased to 10 s for some lines when the depth of penetration of the seismic energy and thickness of the trench sediments became apparent. Sample rate was 1 ms. The MCS geometry is shown in Figure 5.

Marine mammal observers were on deck during all seismic acquisition conducted during daylight hours. There were numerous sightings during the cruise that required turning off the airguns (Table 2). When airgun shut-downs were less than 10 minutes long, we generally simply continued along the profile and resumed shooting when the area was clear, leaving gaps in the data. For longer shut-downs, we turned and filled the gap once shooting could resume. In all, there were 110 separate sightings of 265 individual animals during the cruise (Table 3). The most commonly sighted mammals where fur seals. A number of whales and dolphins were also seen.

Figure 5a. MCS geometry for 48-channel acquisition.

SIO Portable Marine Seismic System

Geometry 1

Cruise: **MV1206**
Vessel: **R/V Melville**
Date: **May 4 – May 19, 2012**
Chief Sci: **A. Trehu**

Techs:
Lee Ellett eellett@ucsd.edu
Jay Turnbull jturnbull@ucsd.edu

Item or Channel	Distance (m) from Stern	Distance (m) from Source	Distance (m) From GPS	Distance (m) off center line	Depth/Height from water
1	111.25	86.25	140.51	3.281 (STBD)	3-4
48	698.75	673.75	728.01	3.281 (STBD)	3-4
Source	25	0	54.26	-3.719 (PORT)	3
GPS	29.26	54.26	0	3.281 (STBD)	0.000

Section	Length (m)	Number of Channels
Towing Cables	105	
Active Sections	600	48
Tail Stretch and Rope	50	
Group Int	12.5	

Source:	GI gun	45/105 True GI	**Qty:**	2
Acq. Sys.	GeoEel	**PreAmp Gain:**	18 db	
Sample Int:	1 ms	**# of Channels:**	48	
File Format:	SEGD	D 8058 Rev 1		
Rec. Length:	9 sec	**Shot Interval:**	25m	

Auxiliary Channels

AUX 1	Gun Timebreak
AUX 2	Gun 1 Near Field
AUX 3	Gun 2 Near Field
AUX 4	Unused

Bird Locations

Bird 1	Start of Tow Stretch	[-104x,3.281y,VARz]
Bird 2	Start of Ch. 1	[-129x,3.281y,VARz]
Bird 3	Start of Ch. 25	[-429x,3.281y,VARz]
Bird 4	Start of Tail Stretch	[-729x,3.281y,VARz]

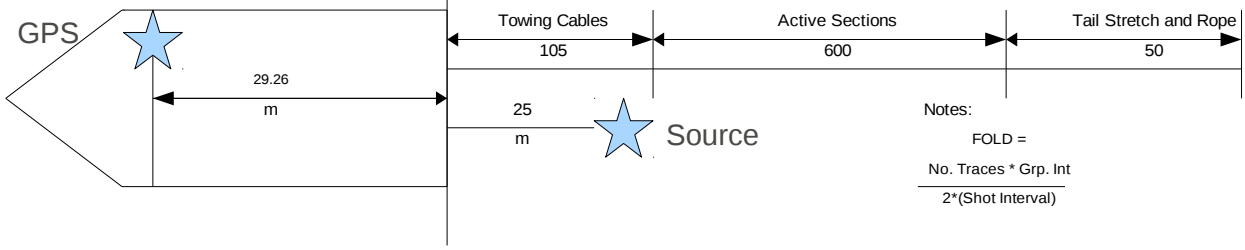

* Not drawn to Scale

Figure 5b. MCS parameters for 40-channel acquisition.

SIO Portable Marine Seismic System

Geometry 1

Cruise: **MV1206**
Vessel: **R/V Melville**
Date: **May 4 – May 19, 2012**
Chief Sci: **A. Trehu**

Techs:
Lee Ellett eellett@ucsd.edu
Jay Turnbull jturnbull@ucsd.edu

Item or Channel	Distance (m) from Stern	Distance (m) from Source	Distance (m) From GPS	Distance (m) off center line	Depth/Height from water
1	111.25	86.25	140.51	3.281 (STBD)	3-4
40	598.75	573.75	628.01	3.281 (STBD)	3-4
Source	25	0	54.26	-3.719 (PORT)	3
GPS	29.26	54.26	0	3.281 (STBD)	0.000

Section	Length (m)	Number of Channels
Towing Cables	105	
Active Sections	500	40
Tail Stretch and Rope	50	
Group Int	12.5	

Source:	GI gun	45/105 True GI	**Qty:**	2
Acq. Sys.	GeoEel	**PreAmp Gain:**	18 db	
Sample Int:	1 ms	**# of Channels:**	40	
File Format:	SEGD	D 8058 Rev 1		
Rec. Length:	9 sec	**Shot Interval:**	25m	

Auxiliary Channels

AUX 1	Gun Timebreak
AUX 2	
AUX 3	
AUX 4	

Bird Locations

Bird 1	Start of Tow Stretch	[-104x,3.281y,VARz]
Bird 2	Start of Ch. 1	[-129x,3.281y,VARz]
Bird 3	Start of Ch. 25	[-429x,3.281y,VARz]
Bird 4	Start of Tail Stretch	[-729x,3.281y,VARz]

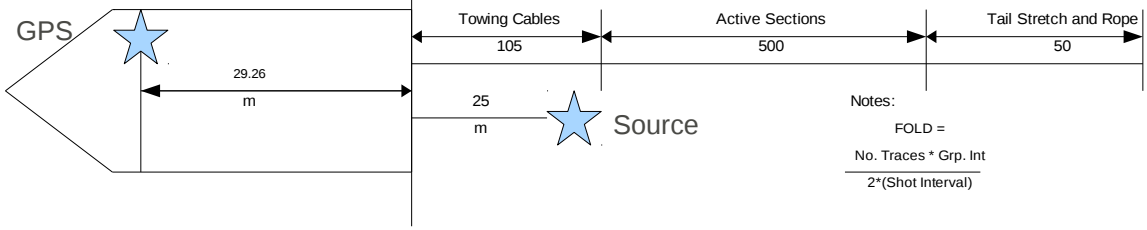

* Not drawn to Scale

Table 2. Times when GI-guns were turned on and off.

Date GMT(yymmdd)	Start GMT	End GMT	Tot time (Hr:min)	Latitude S	Longitude W	Distance Traveled NM	#guns	Comments
12-05-07	13:43		00:33	34 24.10	073 23.79		1	1 gun on
12-05-07		14:16		34 326.06	073 24.74		0	gun off, compressor down
12-05-07	15:28		01:24	34 30.65	073 26.20		1	1 gun firing
12-05-07	15:36		01:16	34 30.43	073 26.88		2	2nd gun firing
12-05-07		16:52		34 25.06	073 24.82			guns off
12-05-07	17:15		03:58	34 24.16	073 24.34		1	1 gun on
12-05-07	17:21		03:52	34 23.79	073 24.16		2	2nd gun on
12-05-07		21:13		34 15.50	073 21.12		0	guns off; entangled with streamer
12-05-07	22:11		00:35	34 14.19	073 17.03		1	1 gun on
12-05-07	22:16		00:30	34 14.04	073 16.61		2	2nd gun on
12-05-07		22:46		34 13.80	073 14.30		0	guns off, compressor failed
12-05-08	00:00			34 15.49	073 08.88		1	1 gun on
12-05-08	00:05			34 15.61	073 08.52		2	2nd gun on
12-05-08		02:46		34 20.54	073 02.73		0	guns off
12-05-09	22:14		01:02	34 31.98	073 26.90		1	1 gun on
12-05-09	22:20		00:56	34 31.56	073 27.24		2	2nd gun firing
12-05-09		23:16		34 30.55	073 31.11		0	guns off
12-05-10	00:13		13:17	34 29.18	073 35.19		1	1 gun on
12-05-10	00:18		13:12	34 29.00	073 35.74		2	2nd gun on
12-05-10		13:30		34 41.14	072 44.68		0	guns off
12-05-10	14:34			34 44.78	072 45.98		1	1 gun on
12-05-10	14:40			34 44.90	072 46.45		2	2 guns on
12-05-10		18:04		34 39.98	073 02.81		0	guns off
12-05-10	18:41			34 40.22	073 04.28		1	1 gun on
12-05-10	18:46			34 40.39	073 03.76		2	2 guns on
12-05-11		12:40		34 43.12	073 07.05		0	guns off
12-05-11	12:50			34 43.36	073 06.31		2	2 guns on
12-05-11		13:43		34 48.68	073 02.22		0	guns off
12-05-11	13:52			34 44.91	073 01.48		2	2 guns on
12-05-12		12:38		34 51.22	073 26.87		0	guns off
12-05-12	12:42			34 52.08	073 26.59		2	guns on
12-05-12		15:11		34 46.70	073 15.77		0	guns off
12-05-12	15:21			34 46.34	073 15.05		2	2 guns on
12-05-12		16.26		34 44.01	073 10.36		0	guns off
12-05-12	16:30			34 43.86	073 10.06		2	2 guns on
12-05-12		16:33		34 43.79	073 09.93		0	guns off
12-05-12	16:40			34 43.54	073 09.41		2	2 guns on
12-05-12		17:38		34 45.11	073 11.17		0	guns off
12-05-12	17:41			34 45.12	073 11.41		2	2 guns on
12-05-12		21:12		34 37.50	072 57.33		0	guns off
12-05-12	21:19			34 37.29	072 56.90		2	2 guns on
12-05-13		19:21		34 46.82	073 27.67		0	guns off
12-05-13	19:26			34 47.04	073 28.09		2	guns on
12-05-13		20:22		34 50.06	073 30.86		0	guns off
12-05-13	20:27			34 50.30	073 31.05		2	guns on
12-05-13		20:44		34 51.29	073 31.91		0	guns off
12-05-13	20:48			34 51.47	073 32.13		2	guns on
12-05-14		07:30		34 29.74	073 27.25			Guns were shut down before 04:00 local time
12-05-14	09:23			x	x			1st Gun ON; no position logged by bridge or observers
12-05-14	09:29			x	x		2	2nd Gun ON; no position logged by bridge or observers
12-05-14		13:26		34 17.46	073 21.81		0	Guns off for maintenance
12-05-14	14:10			34 15.80	073 22.93		1	1st gun on
12-05-14	14:15			34 15.78	073 23.35		2	2nd gun on
12-05-14		14:37		34 16.78	073 23.40		0	Guns off (turtle in zone)
12-05-14	14:41			34 16.90	073 23.14		2	Guns on
12-05-14		16:15		34 19.54	073 16.21		0	Guns off
12-05-14	16:22			34 19.73	073 15.71		2	Guns on
12-05-14		16:40		34 20.44	073 14.36		0	Guns off
12-05-14	16:48			34 20.44	073 13.82		2	Guns on
12-05-14		17:08		34 21.00	073 12.36		0	Guns off
12-05-14	17:14			34 21.16	073 11.92		2	Guns on
12-05-14		17:54		34 22.28	073 08.99		0	Guns off
12-05-14	17:59			34 22.38	073 08.70		2	Guns on
12-05-14		18:34		34 23.34	073 06.19		0	Guns off
12-05-14	18:39			34 23.49	073 05.80		2	Guns on
12-05-14		19:08		34 24.29	073 03.69		0	Guns off
12-05-14	19:15			34 24.48	073 03.18		2	Guns on
12-05-14		19:18		34 24.56	073 02.97		0	Guns off
12-05-14	19:22			34 24.67	073 02.67		2	Guns on
12-05-15		19:47		34 10.92	073 19.53		0	Guns shut down due to entanglement with streamer
12-05-15	21:26			34 09.54	073 19.53		1	1 gun firing
12-05-15	21:32			34 09.95	073 19.42		2	2 guns on
12-05-16		11:01		34.36.76	073.36.97		0	guns off
12-05-16	11:11			34.36.57	073.37.59		2	guns on
12-05-16		14:12		34.41.20	073.44.18		0	guns off
12-05-16	14:18			34.41.44	073.43.63		2	guns on
12-05-16		14:58		34.42.81	073.40.34		0	guns off
12-05-16	15:12			34.43.27	073.39.24		2	guns on
12-05-16		16:43		34.46.25	073.32.13		0	guns off
12-05-16	17:00			34.46.85	073.30.70		1	gun on
12-05-16	17:07			34 47.12	073 30.15		2	2nd gun on
12-05-17		04:35		34 39.13	073 02.87			guns off; will remain off for the rest of the cruise

Table 3. Summary of marine mammal observations.

	Animal Information							GMT Date & Time		Ship and Position Information			
	Sighting Number	Sighting Cue	Species	Group Size	Age	Size	Sex	Yr/Mo/Da	Time (GMT)	Latitude	Longitude	Ship Heading	(kts)
Observer	1	mammal	Otaria flavescens	7				2012-05-04	20:03:00	33 02.11S	071 37.32W	63	5.3
228	2	mammal	Otaria flavescens	2				2012-05-04	20:06:00	33 01.80S	071 36.78W	63	5.3
92	3	mammal	Otaria flavescens	1				2012-05-04	20:47:00	32 58.15S	071 39.45W	63	5.3
228	4	blow	Balaenoptera physalus	2		>12m		2012-05-05	12:22:00	34 33.42S	073 10.65W	37	8.7
228	5	mammal	Arctocephalus sp.	3	adult			2012-05-05	12:36:00	34 33.91S	073 08.96W	111	10.8
92	6	mammal	Arctocephalus sp.	1	adult			2012-05-05	13:06:00	34 35.13S	073 03.26W	111	10.8
92	7	mammal	Otaria flavescens	2				2012-05-05	19:31:00	34 40.40S	073 15.22W	258	11.9
800	8	mammal	Arctocephalus sp.	1				2012-05-05	21:08:00	34 39.82S	073 16.01W	288	0.5
228	9	blow	Balaenoptera sp.	1				2012-05-06	13:38:00	34 26.44S	073 30.52W	276	7.5
92	10	mammal	Arctocephalus sp.	3	adult			2012-05-06	13:57:00	34 27.53S	073 27.23W	276	7.5
92	11	mammal	Lissodelphis peronii	2		1.1m		2012-05-06	14:05:00	34 28.01S	073 25.79W	107	9.5
800	12	mammal	Arctocephalus sp.	6				2012-05-06	14:06:00	34 28.06S	073 25.63W	107	9.5
800	13	mammal	Balaenoptera sp.	1		40 ft		2012-05-06	14:16:00	34 28.63S	073 23.89W	107	9.5
800	14	mammal	Arctocephalus sp.	1				2012-05-06	15:05:00	34 30.92S	073 16.95W	107	9.5
re	15	blow	Balaenoptera physalus	1				2012-05-07	11:29:00	34 25.58S	073 25.09W	19	3.8
228	16	blow	Balaenoptera physalus	3		>10m		2012-05-07	12:12:00	34 23.00S	073 23.52W	41	5.7
800	17	blow	Balaenoptera physalus	3	2 adul	adult 60ft; juv		2012-05-07	14:05:00	34 25.46S	073 24.42W	201	3.9
92	18	blow	Balaenoptera sp.	1				2012-05-07	14:51:00	34 28.66S	073 24.77W	201	3.9
800	19	blow	Balaenoptera sp.	1				2012-05-07	15:34:00	34 30.54S	073 26.69W	241	3.9
228	20	blow	Balaenoptera physalus	2		>10m		2012-05-07	17:31:00	34 23.18S	073 23.84W	42	3.9
800	21	mammal	Arctocephalus sp.	1				2012-05-08	21:27:00	34 40.32S	073 02.17W	286	9.7
800	22	blow	Balaenoptera sp.	2				2012-05-09	12:57:00	34 37.91S	073 09.60W	134	0.0
800	23	blow	Balaenoptera sp.	1				2012-05-09	14:50:00	34 37.90S	073 09.50W	159	0.0
92	24	blow	Balaenoptera physalus	2		50-60 ft		2012-05-09	15:22:00	34 38.00S	073 10.51W	159	0.0
99	25	blow	Balaenoptera physalus	1				2012-05-09	15:59:00	34 38.29S	073 10.85W	202	9.3
228	26	mammal	Arctocephalus sp.	3				2012-05-09	16:03:00	34 35.16S	073 17.57W	5	0.4
800	27	blow	Physeter macrocephalus	2		40 ft		2012-05-09	19:29:00	34 35.17S	073 17.49W	38	0.0
92	28	mammal	Arctocephalus sp.	1				2012-05-09	20:55:00	34 33.64S	073 21.99W	17	9.3
228	29	blow	Balaenoptera sp.	1				2012-05-09	21:06:00	34 33.33S	073 22.90W	17	9.3
228	30	mammal	Arctocephalus sp.	1				2012-05-10	12:06:00	34 39.50S	072 51.15W	120	3.9
228	31	splash	Unid. Dolphin	25				2012-05-10	13:37:00	34 42.19S	072 44.47W	114	4.0
92	32	mammal	Arctocephalus sp.	2				2012-05-10	16:53:00	34 41.88S	072 56.72W	294	4.4
228	33	mammal	Arctocephalus sp.	4				2012-05-10	18:04:00	34 40.09S	073 02.25W	286	4.3
92	34	mammal	Arctocephalus sp.	1				2012-05-10	18:37:00	34 40.05S	073 04.52W	208	4.4
800	35	mammal	Arctocephalus sp.	4	adults			2012-05-10	20:38:00	34 38.66S	073 06.31W	296	4.0
228	36	mammal	Arctocephalus sp.	3				2012-05-10	21:45:00	34 36.86S	073 11.80W	291	4.5
92	37	mammal	Arctocephalus sp.	3				2012-05-11	12:12:00	34 42.40S	073 09.27W	113	4.1
800	38	mammal	Unid. Pinniped	2				2012-05-11	12:18:00	34 42.54S	073 08.86W	113	4.1
800	39	mammal	Arctocephalus sp.	3	2ads/1juv			2012-05-11	12:21:00	34 42.62S	073 08.61W	113	4.1
800	40	mammal	Arctocephalus sp.	1				2012-05-11	13:42:00	34 44.67S	073 02.27W	103	4.4
92	41	mammal	Arctocephalus sp.	1				2012-05-12	12:38:00	34 52.23S	073 26.90W	63	4.1
800	42	mammal	Arctocephalus sp.	1				2012-05-12	15:10:00	34 46.74S	073 15.87W	63	4.0
92	43	mammal	Arctocephalus sp.	2				2012-05-12	15:55:00	34 45.13S	073 12.63W	54	4.4
228	44	mammal	Arctocephalus sp.	2				2012-05-12	16:26:00	34 44.06S	073 10.48W	54	4.4
228	45	mammal	Arctocephalus sp.	2				2012-05-12	16:33:00	34 43.80S	073 09.96W	54	4.4
228	46	mammal	Arctocephalus sp.	2				2012-05-12	21:12:00	34 37.51S	072 57.36W	61	4.0
228	47	splash	Balaenoptera physalus	2				2012-05-12	21:59:00	34 35.82S	072 53.96W	55	4.7
800	48	mammal	Arctocephalus sp.	2				2012-05-13	12:39:00	34 32.46S	072 58.51W	239	4.2
92	49	mammal	Mirounga leonina	1	imm or female			2012-05-13	13:02:00	34 33.28S	073 00.15W	239	4.2
92	50	mammal	Unid. Pinniped	4				2012-05-13	13:34:00	34 34.40S	073 02.44W	239	4.2
92	51	mammal	Arctocephalus sp.	3				2012-05-13	13:50:00	34 34.98S	073 03.61W	239	4.2
92	52	blow	Balaenoptera sp.	4				2012-05-13	17:04:00	34 42.25S	073 17.57W	238	4.3
92	53	blow	Balaenoptera sp.	1				2012-05-13	18:10:00	34 44.23S	073 22.39W	238	4.3
92	54	blow	Balaenoptera physalus	3				2012-05-13	18:13:00	34 44.33S	073 22.60W	238	4.3
92	55	mammal	Arctocephalus sp.	1				2012-05-13	18:26:00	34 44.81S	073 23.58W	238	4.3
92	56	mammal	Arctocephalus sp.	5				2012-05-13	18:53:00	34 45.78S	073 25.57W	234	4.9
800	57	mammal	Arctocephalus sp.	1				2012-05-13	20:22:00	34 50.04S	073 30.83W	216	4.0
228	58	mammal	Arctocephalus sp.	2				2012-05-13	20:44:00	34 51.23S	073 31.92W	216	4.0
228	59	mammal	Unid Small Whale	1				2012-05-14	12:02:00	34 22.54S	073 24.38W	27	3.4
800	60	mammal	Arctocephalus sp.	1				2012-05-14	12:46:00	34 19.88S	073 23.04W	32	4.8
92	61	mammal	Unid. Pinniped	1				2012-05-14	13:05:00	34 18.72S	073 22.46W	24	3.7
92	62	mammal	Arctocephalus sp.	1				2012-05-14	14:01:00	34 16.00S	073 22.44W	300	3.1
228	63	mammal	Arctocephalus sp.	1				2012-05-14	14:09:00	34 15.83S	073 22.84W	300	3.1
228	64	mammal	Arctocephalus sp.	1				2012-05-14	14:14:00	34 15.83S	073 23.22W	265	4.2
92	65	mammal	Arctocephalus sp.	1				2012-05-14	14:36:00	34 16.73S	073 23.52W	16	4.3
228	66	mammal	Arctocephalus sp.	1				2012-05-14	15:27:00	34 18.19S	073 19.77W	109	4.0
92	67	mammal	Arctocephalus sp.	5				2012-05-14	15:57:00	34 19.03S	073 17.55W	112	4.0
800	68	mammal	Arctocephalus sp.	1				2012-05-14	16:01:00	34 19.13S	073 17.28W	112	4.0
800	69	mammal	Arctocephalus sp.	1				2012-05-14	16:07:00	34 19.31S	073 16.83W	112	4.0
800	70	mammal	Arctocephalus sp.	1				2012-05-14	16:11:00	34 19.40S	073 16.57W	112	4.0
92	71	mammal	Arctocephalus sp.	1				2012-05-14	16:13:00	34 19.48S	073 16.38W	112	4.0
92	72	mammal	Arctocephalus sp.	1				2012-05-13	16:22:00	34 19.74S	073 15.69W	112	4.0
92	73	mammal	Arctocephalus sp.	2				2012-05-13	16:25:00	34 19.82S	073 15.48W	112	4.0
92	74	mammal	Arctocephalus sp.	2				2012-05-13	16:51:00	34 20.52S	073 13.61W	112	4.0
92	75	mammal	Arctocephalus sp.	2				2012-05-14	16:53:00	34 20.59S	073 13.45W	112	4.0
92	76	mammal	Arctocephalus sp.	1				2012-05-14	17:08:00	34 21.01S	073 12.33W	111	4.3
800	77	mammal	Arctocephalus sp.	1				2012-05-14	17:11:00	34 21.09S	073 12.11W	111	4.3
800	78	mammal	Arctocephalus sp.	3				2012-05-14	17:12:00	34 21.12S	073 12.05W	111	4.3
800	79	mammal	Arctocephalus sp.	1				2012-05-14	17:31:00	34 21.61S	073 10.75W	111	4.3
92	80	mammal	Arctocephalus sp.	1				2012-05-14	17:37:00	34 21.78S	073 10.31W	111	4.3
92	81	mammal	Arctocephalus sp.	1				2012-05-14	17:48:00	34 22.07S	073 09.53W	111	4.3
92	82	mammal	Arctocephalus sp.	2				2012-05-14	18:05:00	34 22.55S	073 08.27W	121	3.9
92	83	mammal	Arctocephalus sp.	2				2012-05-14	18:20:00	34 22.94S	073 07.24W	121	3.9
92	84	mammal	Arctocephalus sp.	5				2012-05-14	18:22:00	34 23.01S	073 07.07W	121	3.9
92	85	mammal	Arctocephalus sp.	2				2012-05-14	18:40:00	34 23.51S	073 05.76W	115	4.0
228	86	mammal	Arctocephalus sp.	4				2012-05-14	18:46:00	34 23.67S	073 05.31W	115	4.0
228	87	mammal	Arctocephalus sp.	3				2012-05-14	18:49:00	34 23.74S	073 05.12W	115	4.0
228	88	mammal	Arctocephalus sp.	9				2012-05-14	18:56:00	34 23.94S	073 04.62W	115	4.0
228	89	mammal	Arctocephalus sp.	3				2012-05-14	18:58:00	34 24.01S	073 04.41W	115	4.0
228	90	mammal	Arctocephalus sp.	3				2012-05-14	19:11:00	34 24.36S	073 03.50W	115	4.0
228	91	blow	Unid large whale	1				2012-05-15	12:52:00	34 33.08S	073 18.52W	341	4.2
800	92	blow	Unid large whale	1				2012-05-15	13:27:00	34 30.95S	073 19.45W	341	4.2
800	93	blow	Balaenoptera physalus	5				2012-05-16	11:00:00	34 36.84S	073 36.70W	296	3.6
228	94	blow	Balaenoptera physalus	5				2012-05-16	13:20:00	34 38.63S	073 46.29W	239	4.7
92	95	mammal	Arctocephalus sp.	3				2012-05-16	14:56:00	34 42.75S	073 40.51W	123	4.5
800	96	blow	Balaenoptera physalus	2				2012-05-16	15:21:00	34 43.58S	073 38.53W	123	4.5
800	97	blow	Balaenoptera physalus	4				2012-05-16	16:17:00	34 45.39S	073 34.21W	102	4.9
228	98	blow	Balaenoptera sp.	3				2012-05-16	19:17:00	34 47.39S	073 29.40W	98	5.3
800	99	ship	Balaenoptera sp.	1				2012-05-17	11:17:00	34 43.45S	072 39.26W	293	8.8
228	100	blow	Balaenoptera sp.	2				2012-05-17	12:55:00	34 38.48S	072 54.00W	285	8.8
800	101	mammal	Arctocephalus sp.	4				2012-05-17	13:09:00	34 37.76S	072 56.15W	285	8.8
800	102	mammal	Arctocephalus sp.	5				2012-05-17	13:18:00	34 37.35S	072 57.37W	285	8.8
800	103	mammal	Arctocephalus sp.	4				2012-05-17	13:19:00	34 37.28S	072 57.57W	285	8.8
800	104	mammal	Unid. Pinniped	1				2012-05-17	13:35:00	34 36.50S	072 59.89W	285	8.8
800	105	mammal	Arctocephalus sp.	2				2012-05-17	13:56:00	34 35.39S	073 03.18W	285	8.8
800	106	mammal	Arctocephalus sp.	2				2012-05-17	14:08:00	34 34.78S	073 04.97W	285	7.7
92	107	mammal	Arctocephalus sp.	2				2012-05-17	14:13:00	34 34.56S	073 05.63W	285	7.7
92	108	mammal	Balaenoptera sp.	1				2012-05-17	15:10:00	34 31.73S	073 14.03W	285	7.7
92	109	mammal	Arctocephalus sp.	4				2012-05-17	15:25:00	34 30.98S	073 16.31W	285	7.7
92	110	mammal	Arctocephalus sp.	1				2012-05-17	15:47:00	34 29.86S	073 19.56W	285	7.7
92	111	mammal	Arctocephalus sp.	1				2012-05-17	16:46:00	34 26.89S	073 28.37W	288	8.1

Data were processed through frequency-wavenumber (fk) migration using SIOSEIS software. The processing sequence included sorting, normal moveout (NMO), stack, and fk migration. A velocity of 1485 m/s was used for both NMO and migration. In general each line was processed within a few hours of acquisition. Preliminary interpretations of the data guided subsequent acquisition. The complete data set will be available through the Academic Seismic Portal maintained by the University of Texas Institute for Geophysics (http://www.ig.utexas.edu/sdc/) after an initial period of exclusive use by the principle investigators (June, 2014).

Figure 2A shows the location of the MCS lines overlain on the bathymetry; figure 2B identifies the line numbers. Several crossing lines were obtained over each OBS to characterize faults and folds in the study region. When it became apparent that partitioning between sediment accretion and subduction was very variable along this segment of the margin and that there was considerable complex structure beneath the trench sediments, several additional profiles were acquired along the trench and across the deformation front.

Data quality is excellent, due in large part to the broadband source signature (Fig. 6a). Figure 6b shows unfiltered data, illustrating the low frequency nature of the background noise due to waves and the separation between the source signal and background noise. Wave noise varied with sea state, which was variable over the course of the cruise. This example is from a time of relatively rough seas. This low frequency noise could be essentially removed through band-pass filtering. Figure 6c shows data across the deformation front on line 6. The signal from the 2 GI guns penetrates to up to 2 s twtt beneath the seafloor, and the top of the subducted crust can be followed for nearly 10 km landward of the deformation front. On this line, it appears that nearly all of the sediment on the incoming plate is being underthrust, and a possible earlier underthrusting surface can be observed preserved in the accretionary prism. Several additional examples of data can be seen in Appendix 3, which was presented as a poster at the Fall 2012 AGU meeting. The data show a number of interesting features, including complex deposition and erosion in the trench, large and abrupt changes along strike in the amount of sediment that is underthrust beneath the accretionary complex, and the presence of active faulting in the trench and in the accretionary complex.

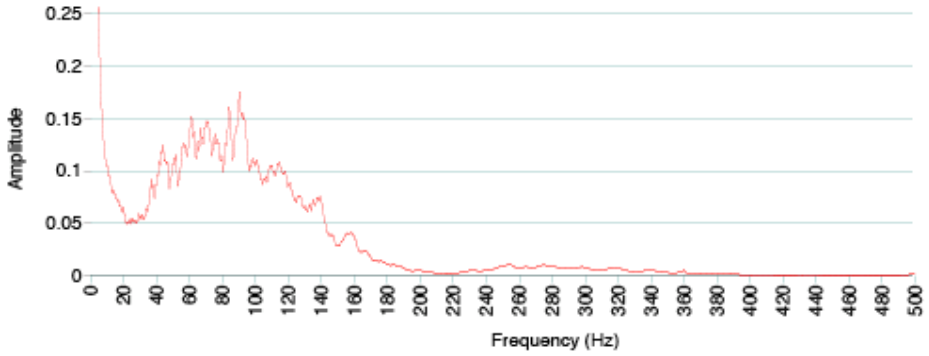

Figure 6a. Amplitude spectrum of data in Figure 6b.

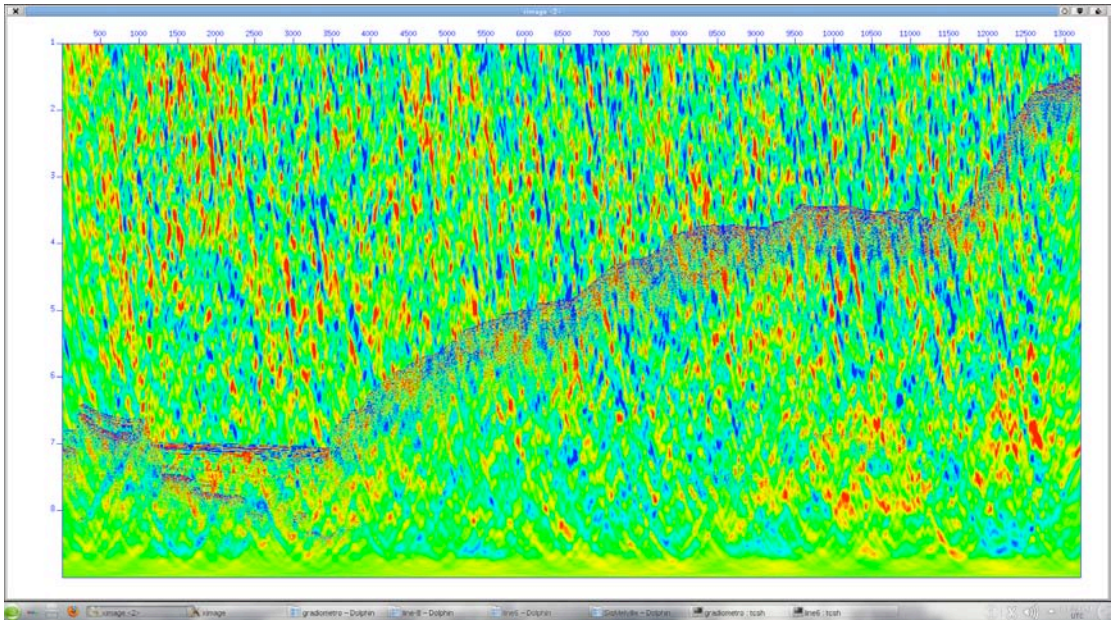

Figure 6b. Data from line 6 without any filtering showing separation between wave-generated noise and the signal from the GI-guns.

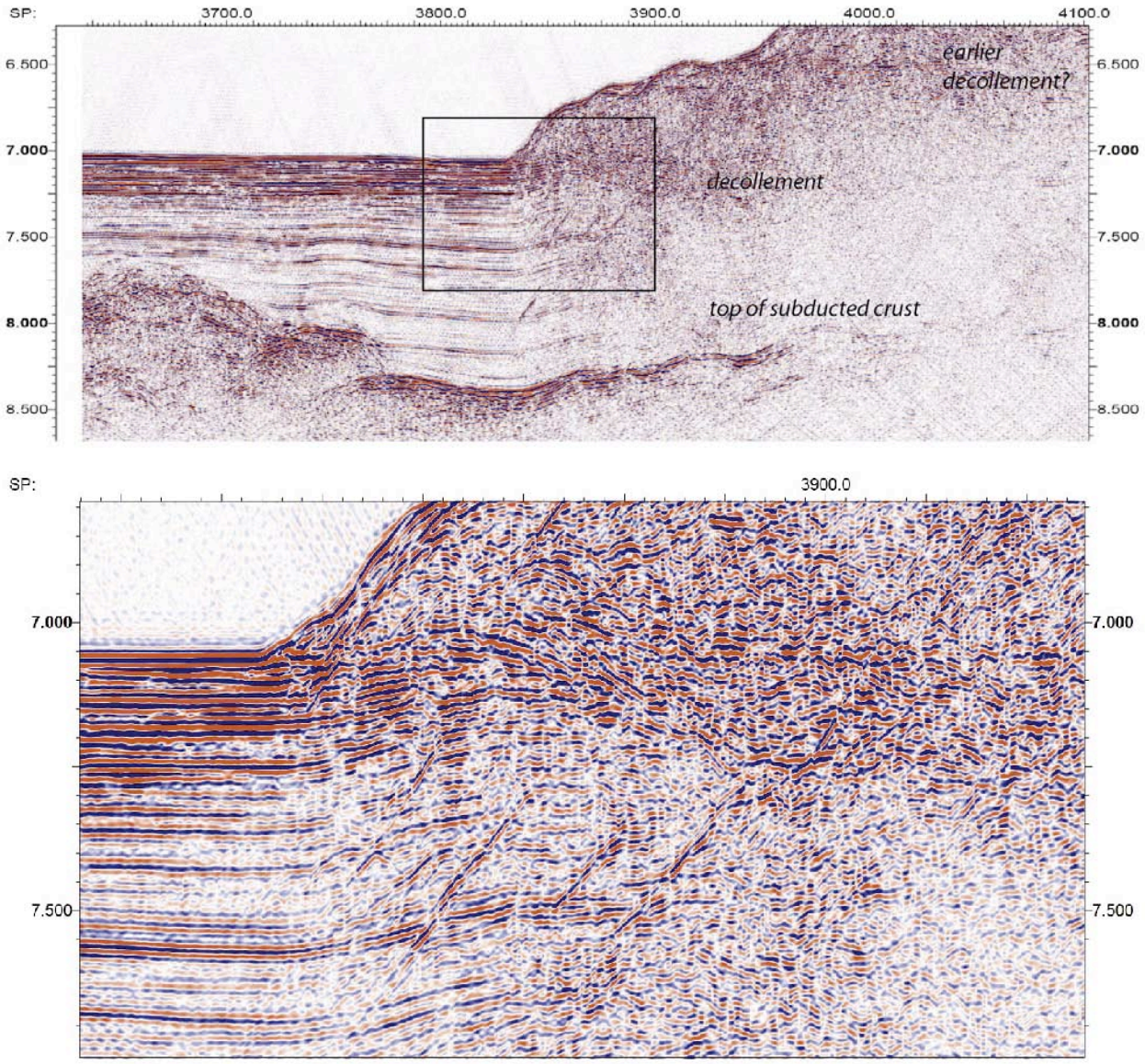

Figure 6c. Portion of line 6 after application of bandpass filtering and f-k migration. The top of the subducted oceanic crust can be seen for ~2000 shots (5 km) landward of the deformation front. A second low frequency reflection can be seen that may be the top of underthrust sediment. The structure of the deformation front varies significantly over very short along-strike distances. Considerable topography, both of constructional and tectonic origin, is seen on the subducting plate.

Expendible BathyThermograph (XBT) data:

XBTs, which measure water temperature in the upper 1000 m of the water column, were acquired at least once per day, with several XBTs acquired on some days in order to provide higher resolution of oceanographic conditions during certain profiles to support attempts to image water column features in the seismic data and for correcting bathymetric data. Data were converted to sound velocity by the onboard software assuming standard salinity. XBT data were acquired at least once per day, with additional data acquired as needed to maintain temporal and spatial coverage. The new profiles were immediately loaded into the EM122 multibeam acquisition software package to maintain its calibration for comparing bathymetry with previously acquired data. Following is a table of time of acquisition and site location for XBT casts and plots of the data. Data can be downloaded from the Rolling Deck to Repository (R2R) web site (http://www.rvdata.us/catalog/MV1206).

Table 4. Locations of XBT profiles.

File	Time	Latitude	Longitude
XBT01	5/4/12 23:23	33° 19.99' S	72° 04.78' W
XBT02	5/5/12 12:00	34° 31.95' S	73° 12.32' W
XBT03	5/6/12 12:44	34° 23.02' S	73° 39.94' W
XBT04	5/6/12 16:03	34° 34.35' S	73° 06.69' W
XBT05	5/6/12 18:21	34° 42.62' S	72° 41.99' W
XBT06	5/7/12 16:30	34° 26.94' S	73° 25.79' W
XBT07	5/8/12 19:06	34° 42.76' S	72° 55.49' W
XBT08	5/9/12 15:54	34° 38.59' S	73° 10.30' W
XBT09	5/10/12 1:55	34° 24.22' S	73° 37.68' W
XBT10	5/10/12 13:06	34° 41.09' S	72° 46.50' W
XBT11	5/10/12 20:35	34° 38.71' S	73° 06.17' W
XBT12	5/10/12 23:52	34° 33.67' S	73° 21.49' W
XBT13	5/11/12 3:09	34° 28.80' S	73° 36.30' W
XBT14	5/11/12 20:53	34° 50.83' S	73° 04.68' W
XBT15	5/12/12 1:03	34° 52.53' S	73° 26.00' W
XBT16	5/12/12 5:17	34° 54.25' S	73° 48.02' W
XBT17	5/12/12 13:08	34° 51.14' S	73° 24.70' W
XBT18	5/12/12 23:17	34° 32.92' S	72° 48.15' W
XBT19	5/14/12 12:49	34° 19.68' S	73° 22.94' W
XBT20	5/14/12 20:31	34° 26.54' S	72° 57.77' W
XBT21	5/15/12 18:46	34° 11.30' S	73° 18.81' W
XBT22	5/16/12 22:14	34° 53.40' S	73° 15.07' W
XBT23	5/17/12 11:06	34° 44.02' S	72° 37.56' W
XBT24	5/17/12 14:02	34° 35.06' S	73° 04.18' W
XBT25	5/17/12 16:13	34° 28.50' S	73° 23.61' W
XBT26	5/17/12 19:10	34° 19.73' S	73° 49.55' W

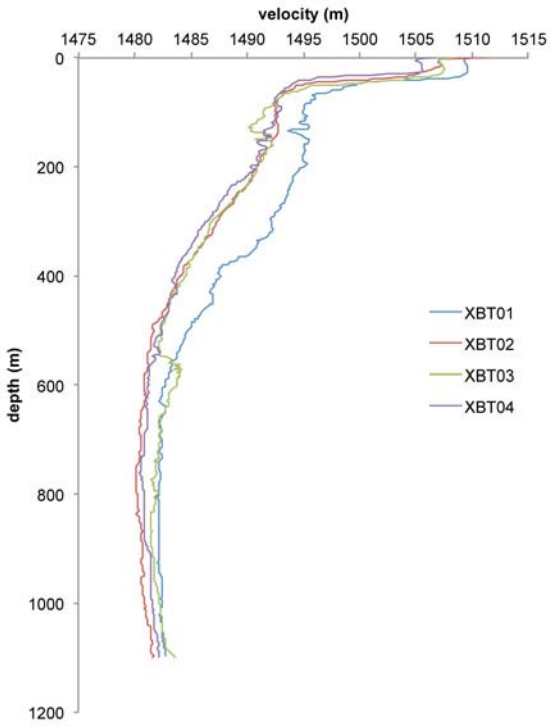
velocity (m)
1475 1480 1485 1490 1495 1500 1505 1510 1515
0 200 400 600 800 1000 1200
depth (m)
XBT01
XBT02
XBT03
XBT04

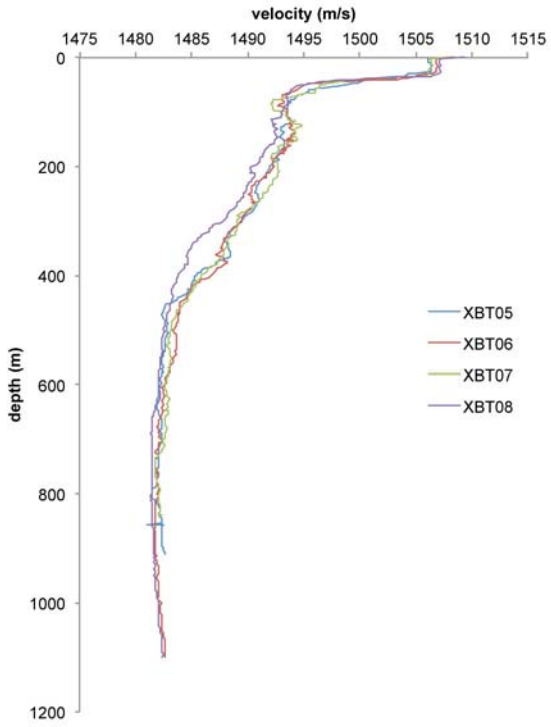
velocity (m/s)
1475 1480 1485 1490 1495 1500 1505 1510 1515
0 200 400 600 800 1000 1200
depth (m)
XBT05
XBT06
XBT07
XBT08

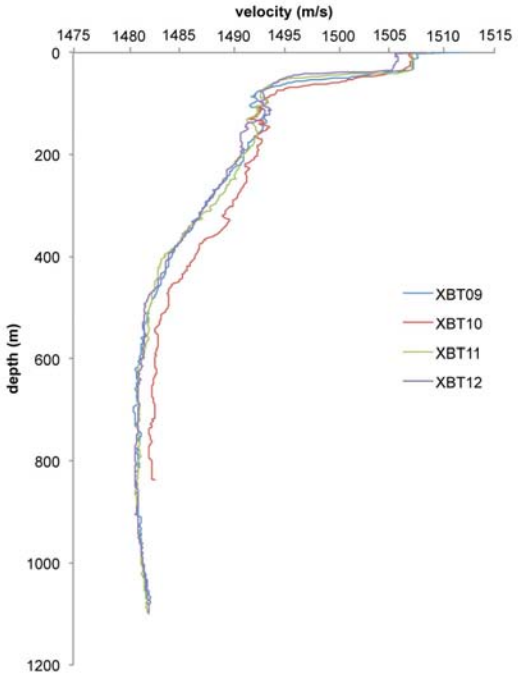
velocity (m/s)
1475 1480 1485 1490 1495 1500 1505 1510 1515
0 200 400 600 800 1000 1200
depth (m)
XBT09
XBT10
XBT11
XBT12

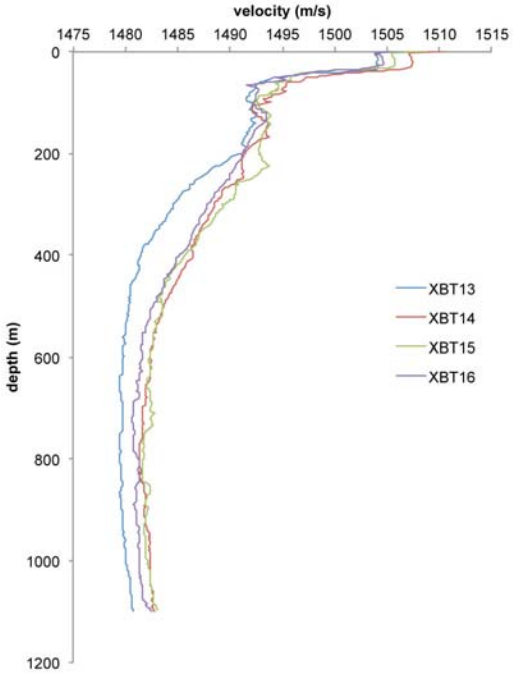
velocity (m/s)
1475 1480 1485 1490 1495 1500 1505 1510 1515
0 200 400 600 800 1000 1200
depth (m)
XBT13
XBT14
XBT15
XBT16

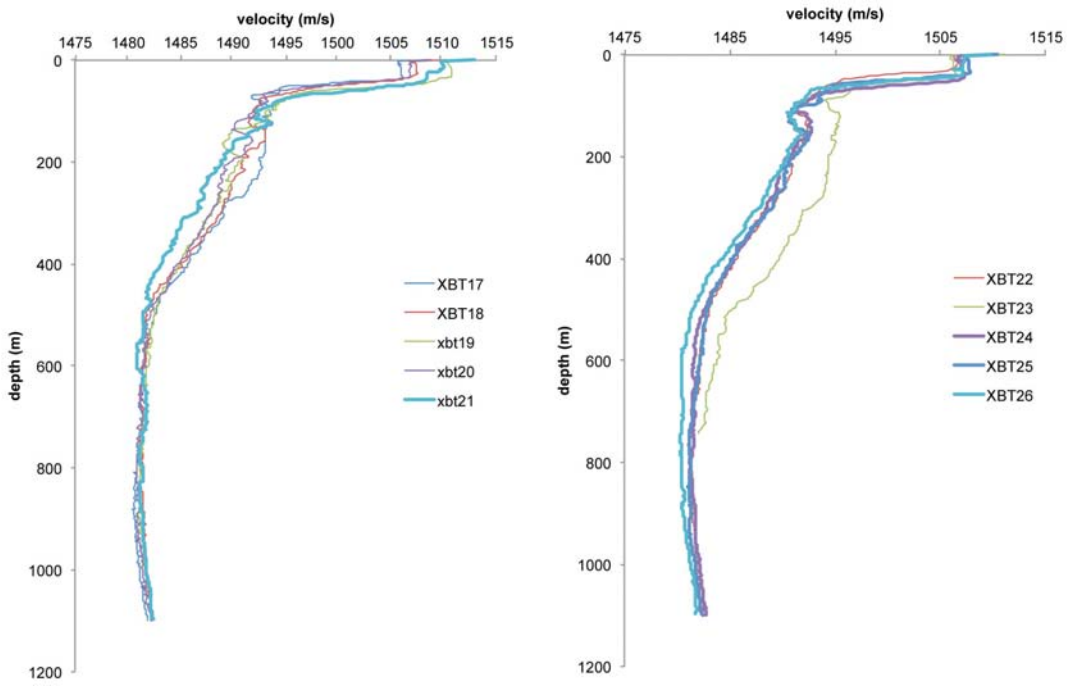

Figure 7. XBT profiles. Site locations are given in Table 2 and are shown in Figure 2b.

EM-122 swath bathymetry:

Kongsberg EM-122 multibeam swath bathymetry data were acquired and processed throughout the cruise (Fig. 2). Data were processed using MBSytem to edit bad pings and generate a grid with 200 m resolution, shown in Figure 2, with a detail from the trench shown in Figure 8. Because of good weather and the relatively slow speed of the ship, data quality in the trench is significantly improved compared to existing data. One longer bathymetric profile across the outer-rise, trench and forearc was acquired for comparison with a profile acquired by Geomar using the HMRV James Cook in 2008 and repeated by Scripps Institution of Oceanography in 2011. XBTs were acquired at least once/day, and more often during the profile intended for comparison with previous data, and the water column velocity was updated to reflect the most recent XBT. A BIST test was run at the end of the previous cruise and confirmed that the EM122 system was operating optimally.

Water column data were saved as well as seafloor depth and reflectivity for most of the cruise. However, this option was turned off late in the cruise when it was suspected that this option was responsible for anomalously frequent system crashes due to memory issues with GridEngine. These required restarting the system several times during the cruise, and starting new surveys, which are designated in the database as MV1206a, MV1206b, etc. Why exercising the option of saving water column data should be problematic was not understood.

Watchstanders were charged with keeping an eye on the screen showing the water column data and with noting any anomalous signals indicative of free gas bubbles venting from the seafloor in the watchstander log. No such events were noted during the MV1206.

Data can be downloaded from the Rolling Deck to Repository (R2R) web site (http://www.rvdata.us/catalog/MV1206).

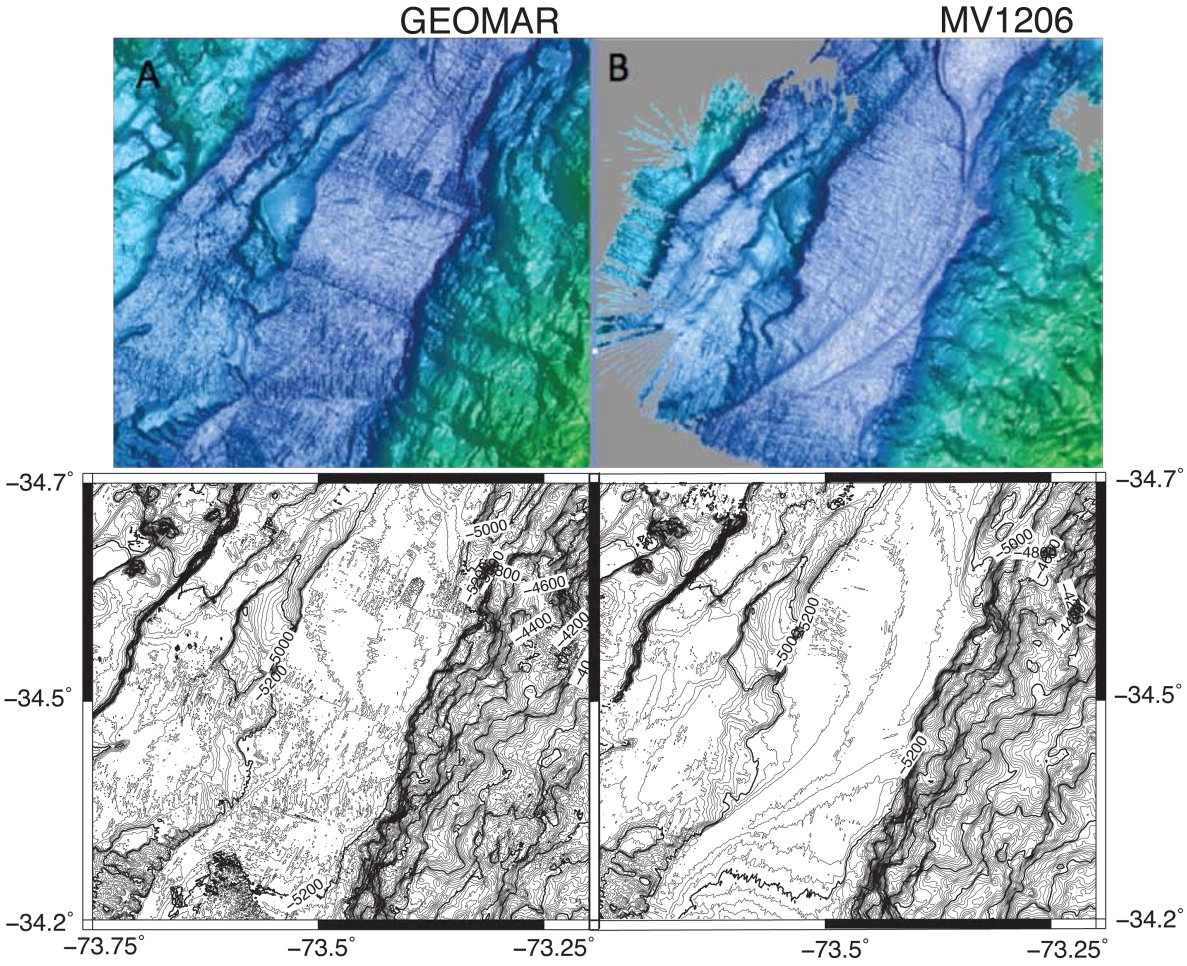

Figure 8. Example of bathymetry in the trench from this cruise (B) compared to bathymetry available from a previous GEOMAR cruise (A). Contour interval is 20 m. While the major features are the same, the new data provide allow us to look at subtle topographic variations in the trench.

Magnetics:

Magnetic anomaly data were acquired both in gradiometer and in single magnetometer mode (Figure 9). Early in the cruise, we ran a "figure of merit" to determine whether the data were affected by the presence of the ship. Although we had originally planned to acquire magnetic data throughout the cruise while acquiring MCS data, this proved to be impossible because the magnetometer cable and GI-guns were getting tangled. Fortunately we were able to untangle them before equipment was damaged. Magnetic data were therefore acquired when the seismic

system was being repaired. Data from SAMBA (South American Magnotometer B-Field Array; see http://samba.atmos.ucla.edu) are available for correcting the data for temporal changes in the magnetic field. A map showing the lines along which magnetic data were acquired is shown in Figure 10. Raw data are shown in Figure 11. Data will be available through NGDC. Data are referenced to time and must be merged with the ship's GPS data. When towed as a gradiometer, the distance between the reported ship position and the first fish is 629m; second fish is 100m behind that. When a single magnetometer was towed, the distance from the ship position to the fish is 329m. Data can be downloaded from the Rolling Deck to Repository (R2R) web site (http://www.rvdata.us/catalog/MV1206).

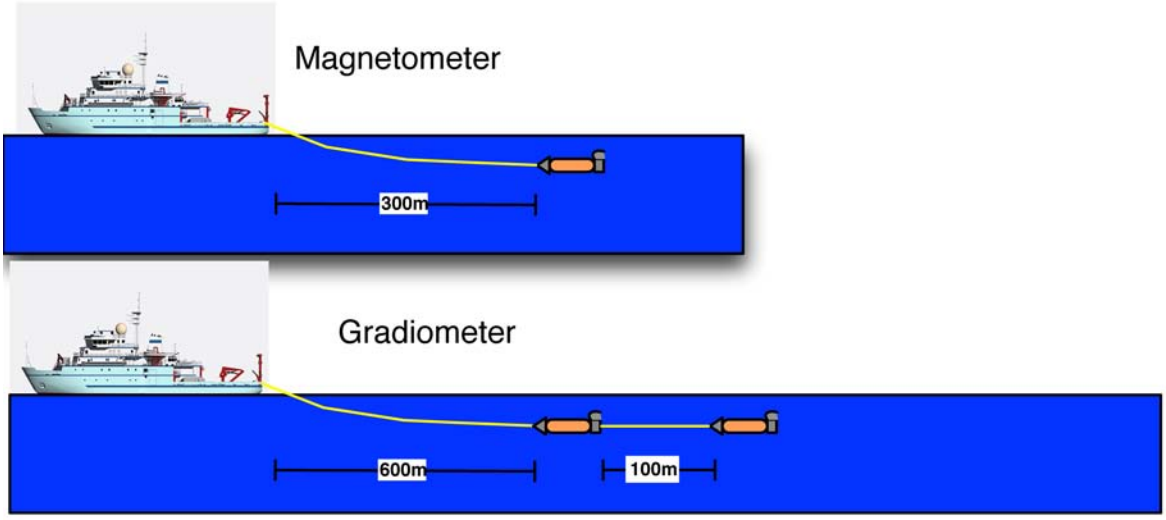

Figure 9. Magnetometer towing diagram.

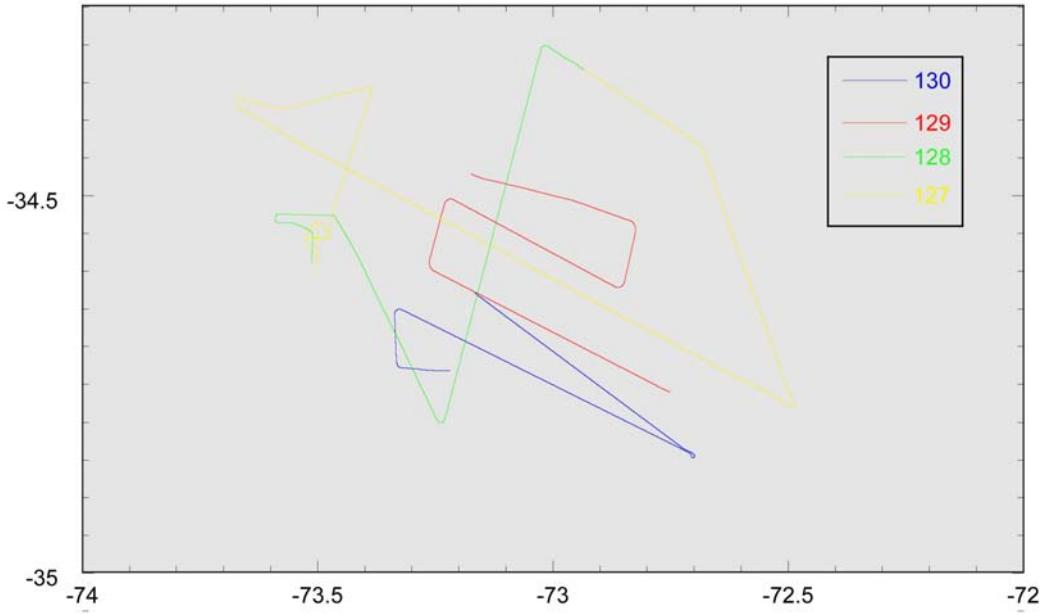

Figure 10. Map showing ship tracks during acquisition of magnetic gradiometer data.

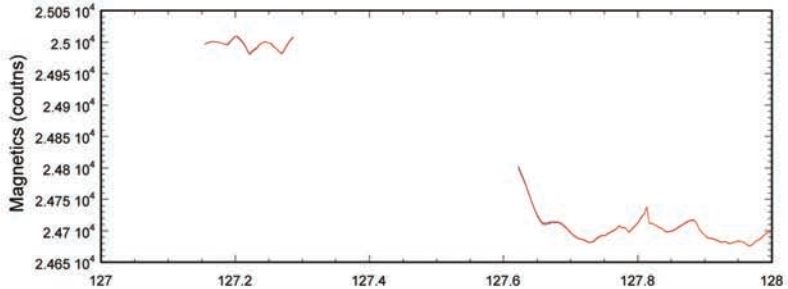
Magnetics (coutns)
2.505 10^4
2.5 10^4
2.495 10^4
2.49 10^4
2.485 10^4
2.48 10^4
2.475 10^4
2.47 10^4
2.465 10^4
127
127.2
127.4
127.6
127.8
128

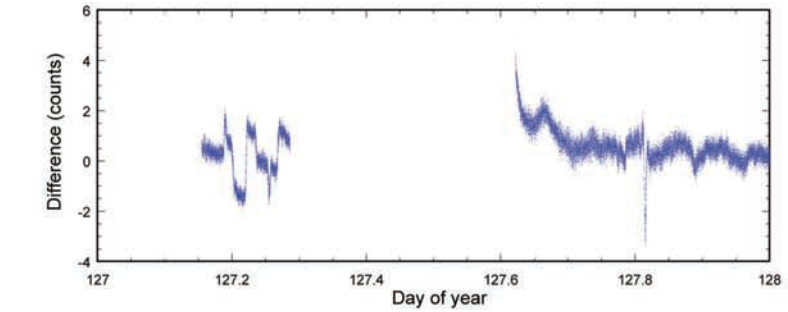
Difference (counts)
6
4
2
0
-2
-4
127
127.2
127.4
127.6
127.8
128
Day of year

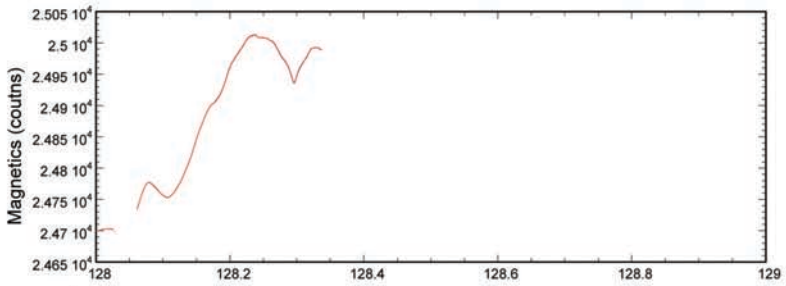
Magnetics (coutns)
2.505 10^4
2.5 10^4
2.495 10^4
2.49 10^4
2.485 10^4
2.48 10^4
2.475 10^4
2.47 10^4
2.465 10^4
128
128.2
128.4
128.6
128.8
129

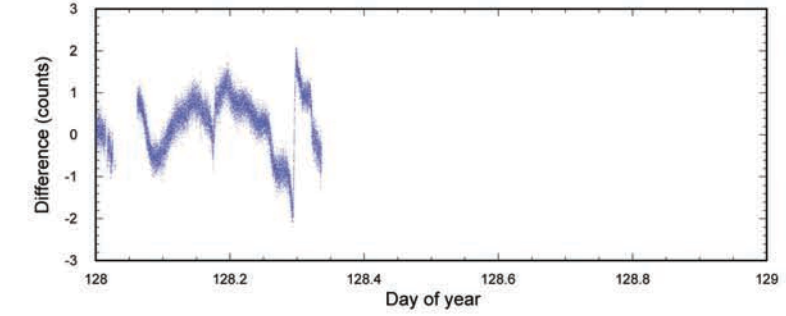
Difference (counts)
3
2
1
0
-1
-2
-3
128
128.2
128.4
128.6
128.8
129
Day of year

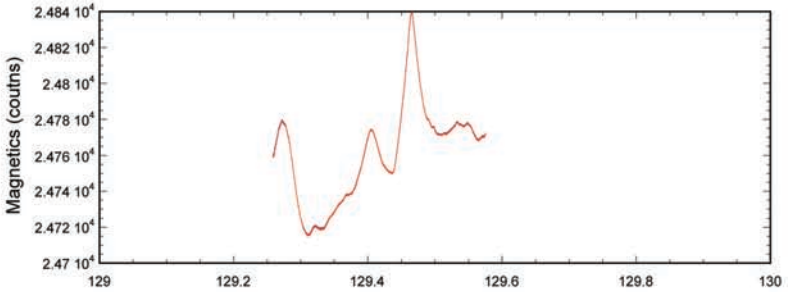
Magnetics (coutns)
2.484 10^4
2.482 10^4
2.48 10^4
2.478 10^4
2.476 10^4
2.474 10^4
2.472 10^4
2.47 10^4
129
129.2
129.4
129.6
129.8
130

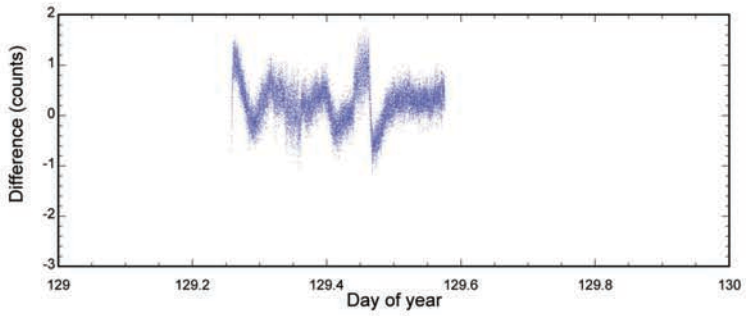
Difference (counts)
2
1
0
-1
-2
-3
129
129.2
129.4
129.6
129.8
130
Day of year

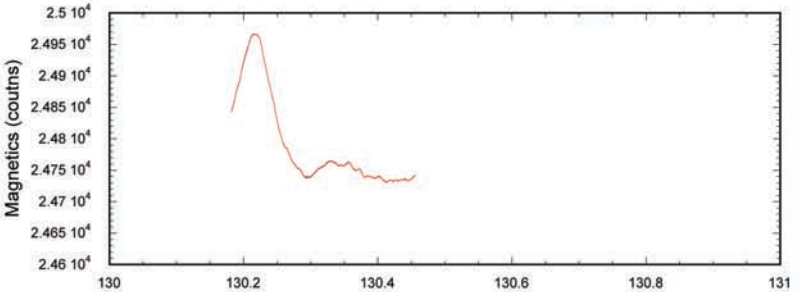
Magnetics (coutns)
2.5 10^4
2.495 10^4
2.49 10^4
2.485 10^4
2.48 10^4
2.475 10^4
2.47 10^4
2.465 10^4
2.46 10^4
130
130.2
130.4
130.6
130.8
131

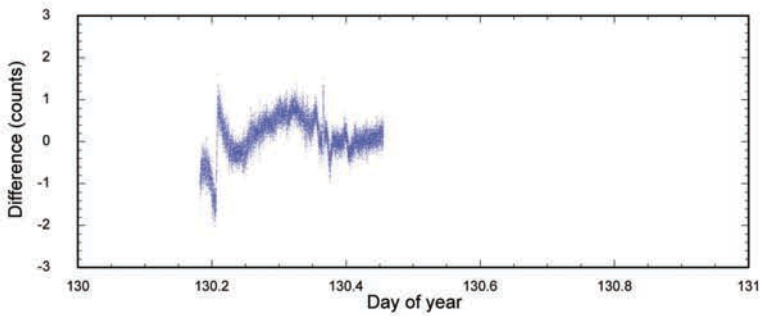
Difference (counts)
3
2
1
0
-1
-2
-3
130
130.2
130.4
130.6
130.8
131
Day of year

Figure 11. Magnetic data. The raw data recorded on each magnetometer and the difference between the two magnetometers is shown.

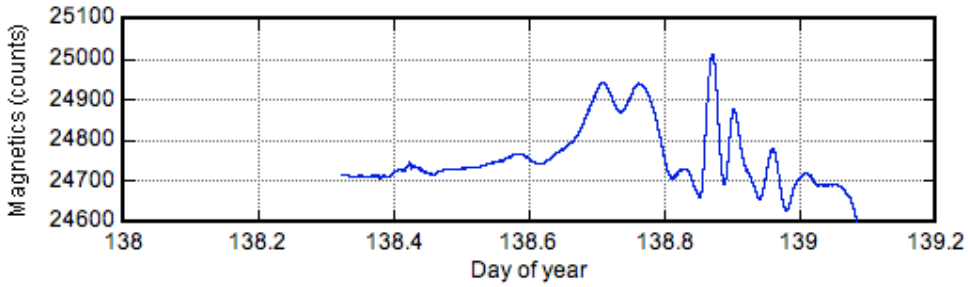

Figure 12. Magnetic data from May 17 and 18. Only a single magnetometer acquired data during this time period.

Gravity:

Gravity data were acquired throughout the cruise, with the exception of a 2.5 hour period on May 12. Raw data are shown in Figure 12. Gravity ties were taken at a base station in Valparaiso, Chile, immediately before and after the cruise (Table 3). However, after the computer crash on May 12, corrections were applied from the previous cruise (Puenta Arenas, Chile on March 20, 2012). Data can be downloaded from the Rolling Deck to Repository (R2R) web site (http://www.rvdata.us/catalog/MV1206).

UTC TIE DATE: 2012/04/20 16:20:34.426	UTC TIE DATE: 2012/05/01 15:39:54.628	UTC TIE DATE: 2012/05/18 16:34:19.929
Ship: R/V Melville	Ship: R/V Melville	Ship: R/V Melville
Personnel: Cohen,Meyer	Personnel: Meyer	Personnel: Meyer, Hale
Port/Pier/Berth: Punta Arenas, Chile Mardones (sp?) pier	Port/Pier/Berth:Valpariso/Pier1/Berth 7	Port/Pier/Berth: Valparaiso/Pier7
Gravity station number: DOD 0216-5/WH1019/IGB 51230 N	Gravity station number: 0048.09	Gravity station number: PFPE 2010.01
Station name: PUNTA ARENAS	Station name: Pier 1 - Berth 4	Station name: Valpo Pier 7
mGal at pier: 981304.97299952	mGal at pier: 979618.732	mGal at pier: 979618.732
Water height to pier 1: 11.416	Water height to pier 1: 9.916	Water height to pier 1: 9.083
Water height to pier 2: 11.5	Water height to pier 2: 10.25	Water height to pier 2: 9. 318
Water height to pier 3: 11	Water height to pier 3: 10.75	Water height to pier 3: 9.166
Average filtered counts: 25285.095180833	Average filtered counts: 24944.902421111	Average filtered counts: 24944.905703889
Filter length: 181	Filter length: 361	Filter length: 181
Scale factor: 4.9826266	Scale factor: 4.9826266	Scale factor: 4.9826266
New bias: 855319.8478693	New bias: 855328.5663635	New bias: 855328.15310731

Table 5. Gravity base station data.

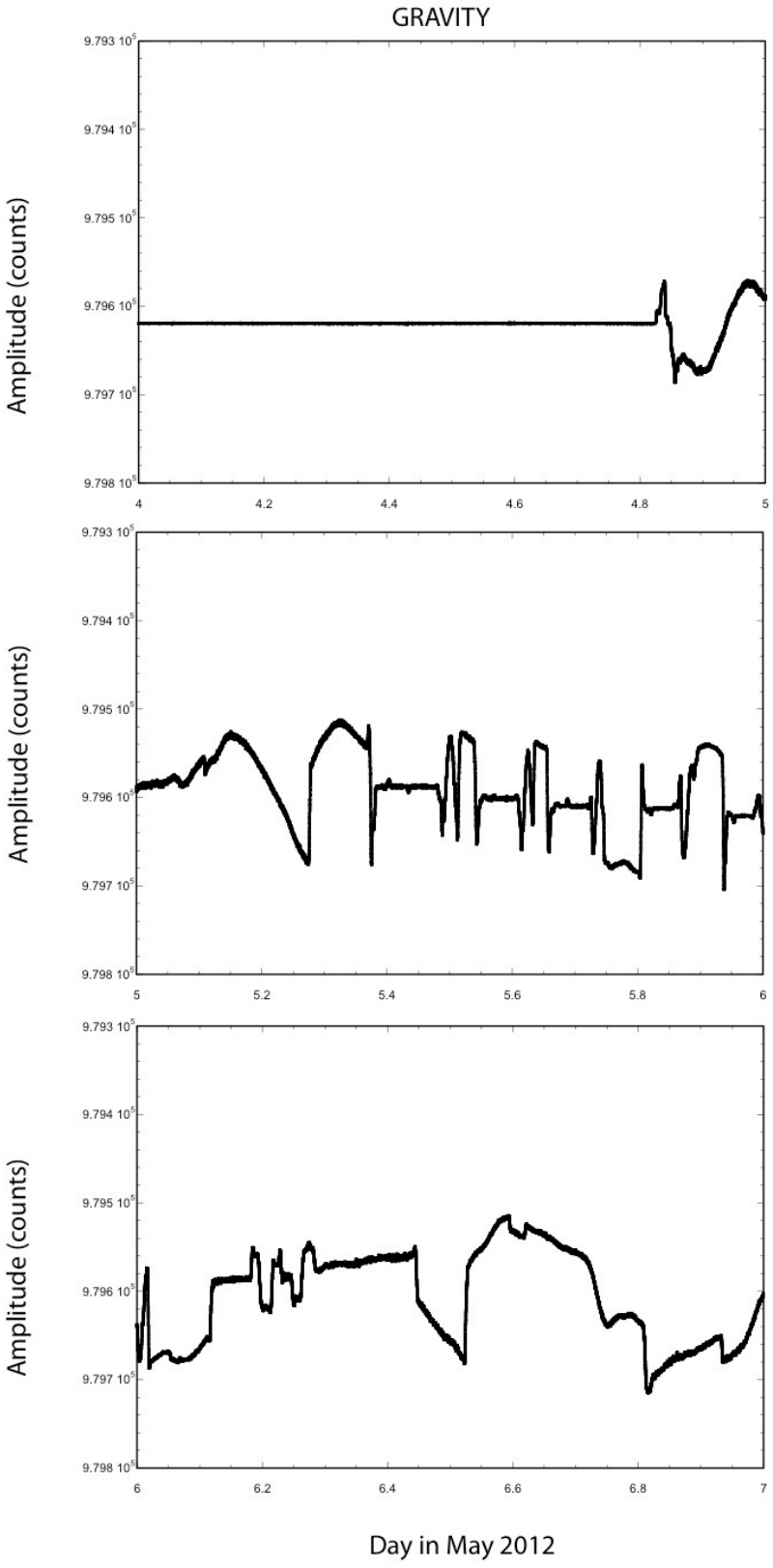
GRAVITY
Amplitude (counts)
9.793 10^5
9.794 10^5
9.795 10^5
9.796 10^5
9.797 10^5
9.798 10^5
4
4.2
4.4
4.6
4.8
5
Amplitude (counts)
5
5.2
5.4
5.6
5.8
6
Amplitude (counts)
6
6.2
6.4
6.6
6.8
7
Day in May 2012

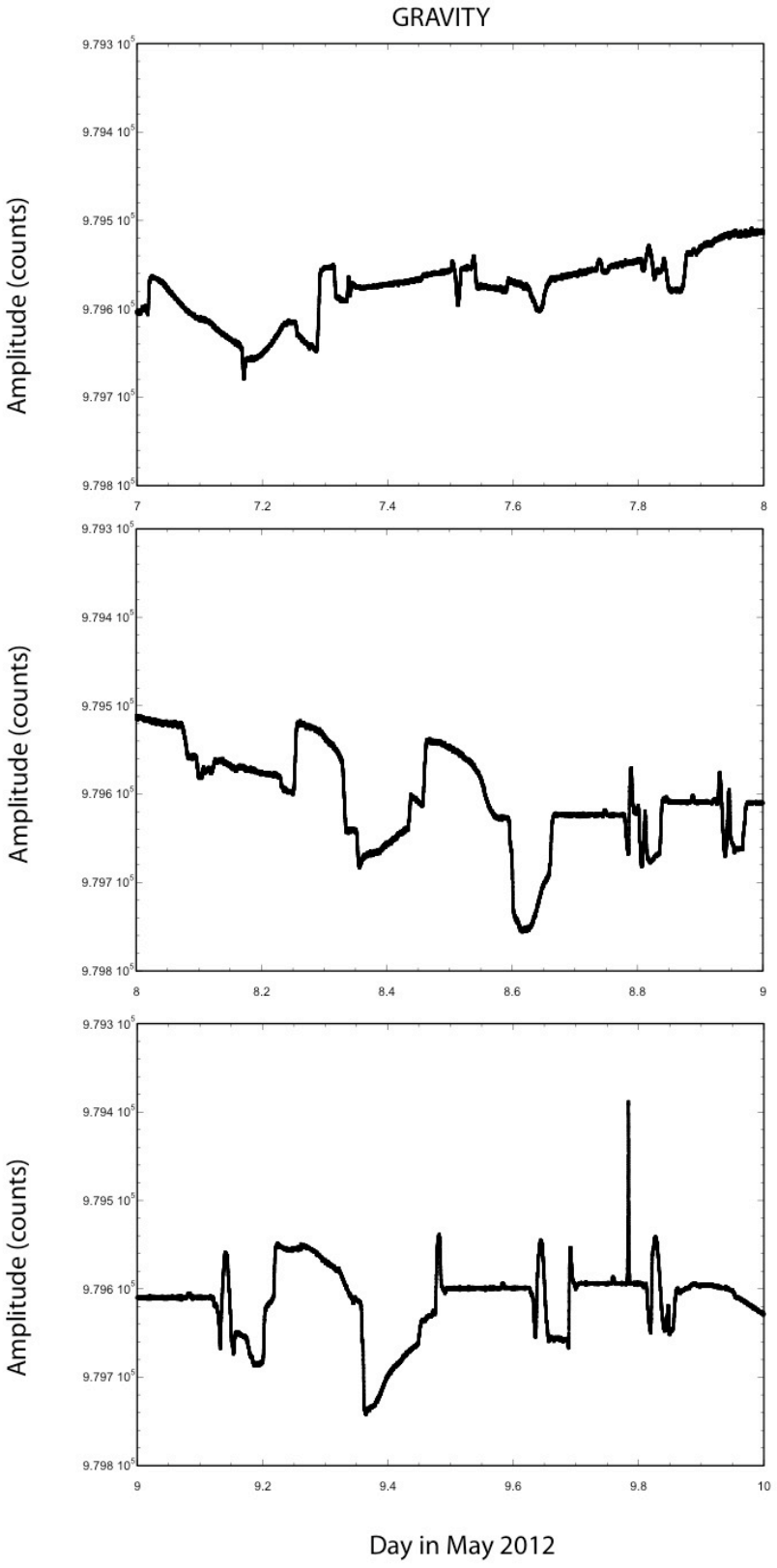
GRAVITY
Amplitude (counts)
9.793 10^5
9.794 10^5
9.795 10^5
9.796 10^5
9.797 10^5
9.798 10^5
7
7.2
7.4
7.6
7.8
8
Amplitude (counts)
9.793 10^5
9.794 10^5
9.795 10^5
9.796 10^5
9.797 10^5
9.798 10^5
8
8.2
8.4
8.6
8.8
9
Amplitude (counts)
9.793 10^5
9.794 10^5
9.795 10^5
9.796 10^5
9.797 10^5
9.798 10^5
9
9.2
9.4
9.6
9.8
10
Day in May 2012

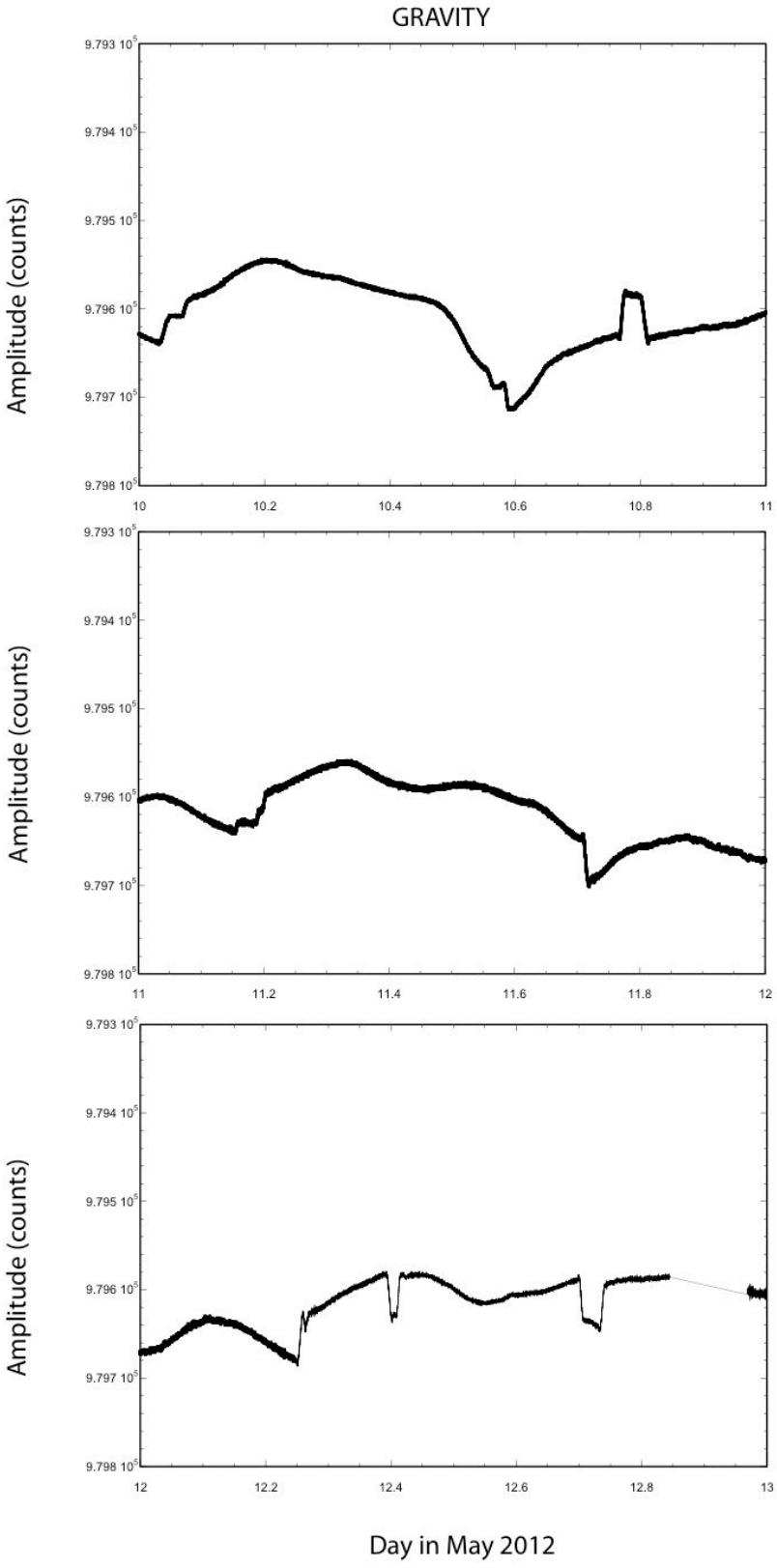
GRAVITY
Amplitude (counts)
9.793 10^5
9.794 10^5
9.795 10^5
9.796 10^5
9.797 10^5
9.798 10^5
10
10.2
10.4
10.6
10.8
11
Amplitude (counts)
11
11.2
11.4
11.6
11.8
12
Amplitude (counts)
12
12.2
12.4
12.6
12.8
13
Day in May 2012

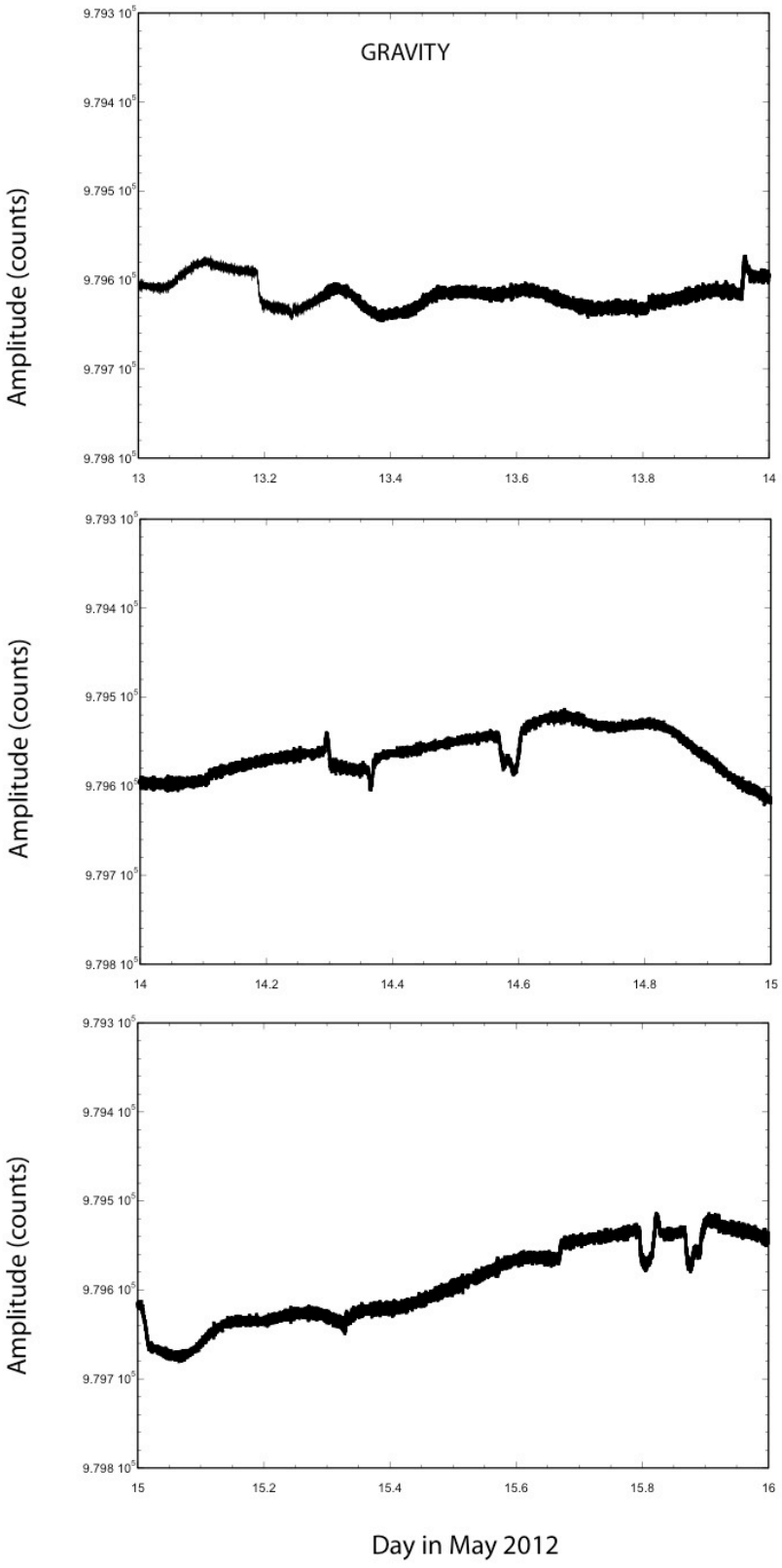
GRAVITY
Amplitude (counts)
9.793 10^5
9.794 10^5
9.795 10^5
9.796 10^5
9.797 10^5
9.798 10^5
13
13.2
13.4
13.6
13.8
14
Amplitude (counts)
9.793 10^5
9.794 10^5
9.795 10^5
9.796 10^5
9.797 10^5
9.798 10^5
14
14.2
14.4
14.6
14.8
15
Amplitude (counts)
9.793 10^5
9.794 10^5
9.795 10^5
9.796 10^5
9.797 10^5
9.798 10^5
15
15.2
15.4
15.6
15.8
16
Day in May 2012

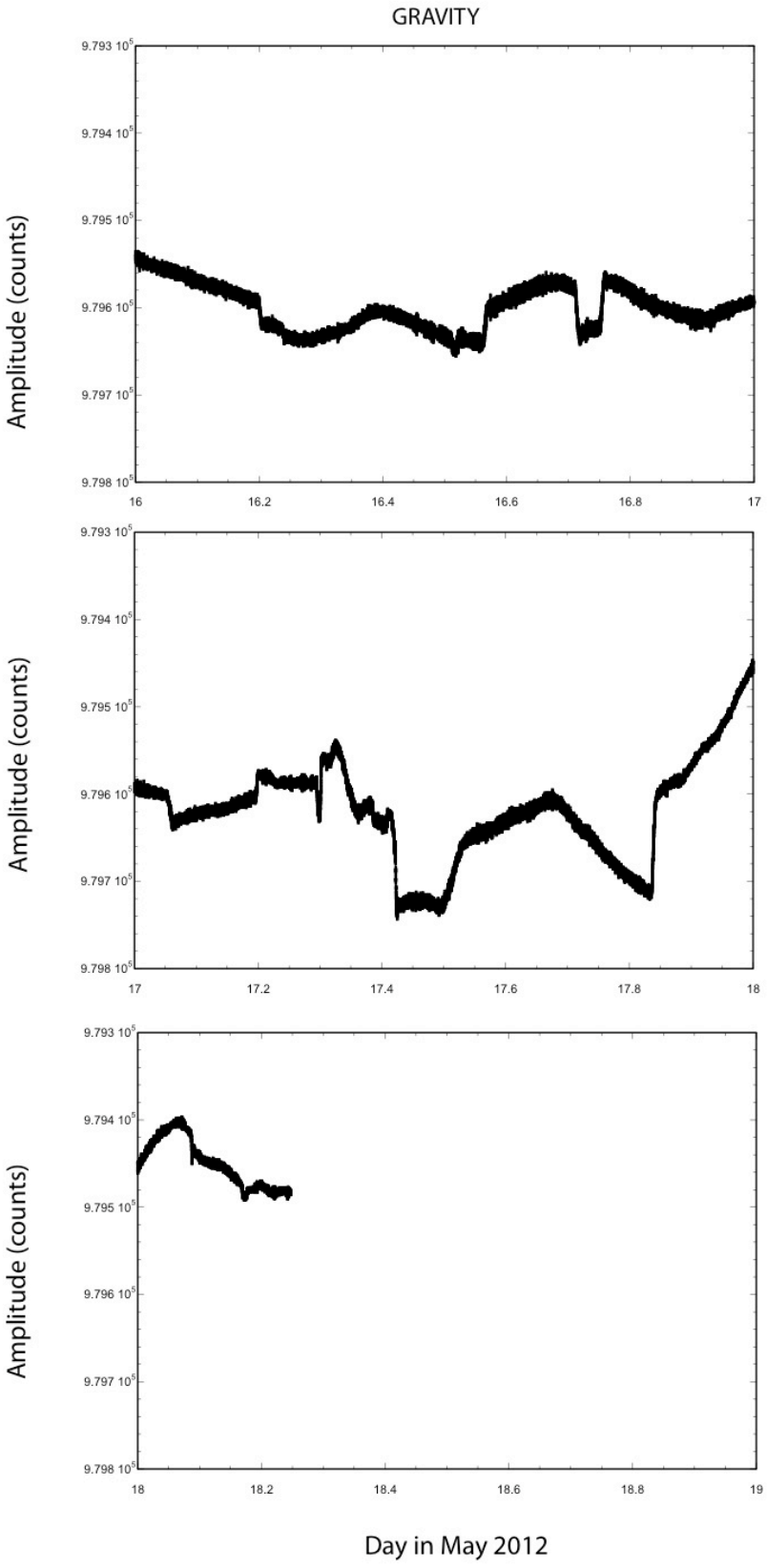
GRAVITY
Amplitude (counts)
9.793 10^5
9.794 10^5
9.795 10^5
9.796 10^5
9.797 10^5
9.798 10^5
16
16.2
16.4
16.6
16.8
17
Amplitude (counts)
9.793 10^5
9.794 10^5
9.795 10^5
9.796 10^5
9.797 10^5
9.798 10^5
17
17.2
17.4
17.6
17.8
18
Amplitude (counts)
9.793 10^5
9.794 10^5
9.795 10^5
9.796 10^5
9.797 10^5
9.798 10^5
18
18.2
18.4
18.6
18.8
19
Day in May 2012

Acoustic Doppler Current Profiler (ADCP):

ADCP data were acquired throughout the cruise at the 75 kHz. Data were processed during the cruise using University of Hawaii UHDAS software. A few example plots from the plot archive are shown in Figure 13. For each day of the cruise, the archive includes map views of shallow current speed, direction and sea surface temperature, and of the north-south and east-west components of the current as a function of depth versus time, latitude and longitude (i.e. 4 plots/day for 75nb and 4 for 75bb). The raw data, plot archive, and reprocessed data are available from the from Joint Archive for Shipboard ADCP data at the University of Hawaii (ilikai.soest.hawaii.edu/sadcp/) or from the R2R web site (www.rvdata.us/catalog/MV1206).

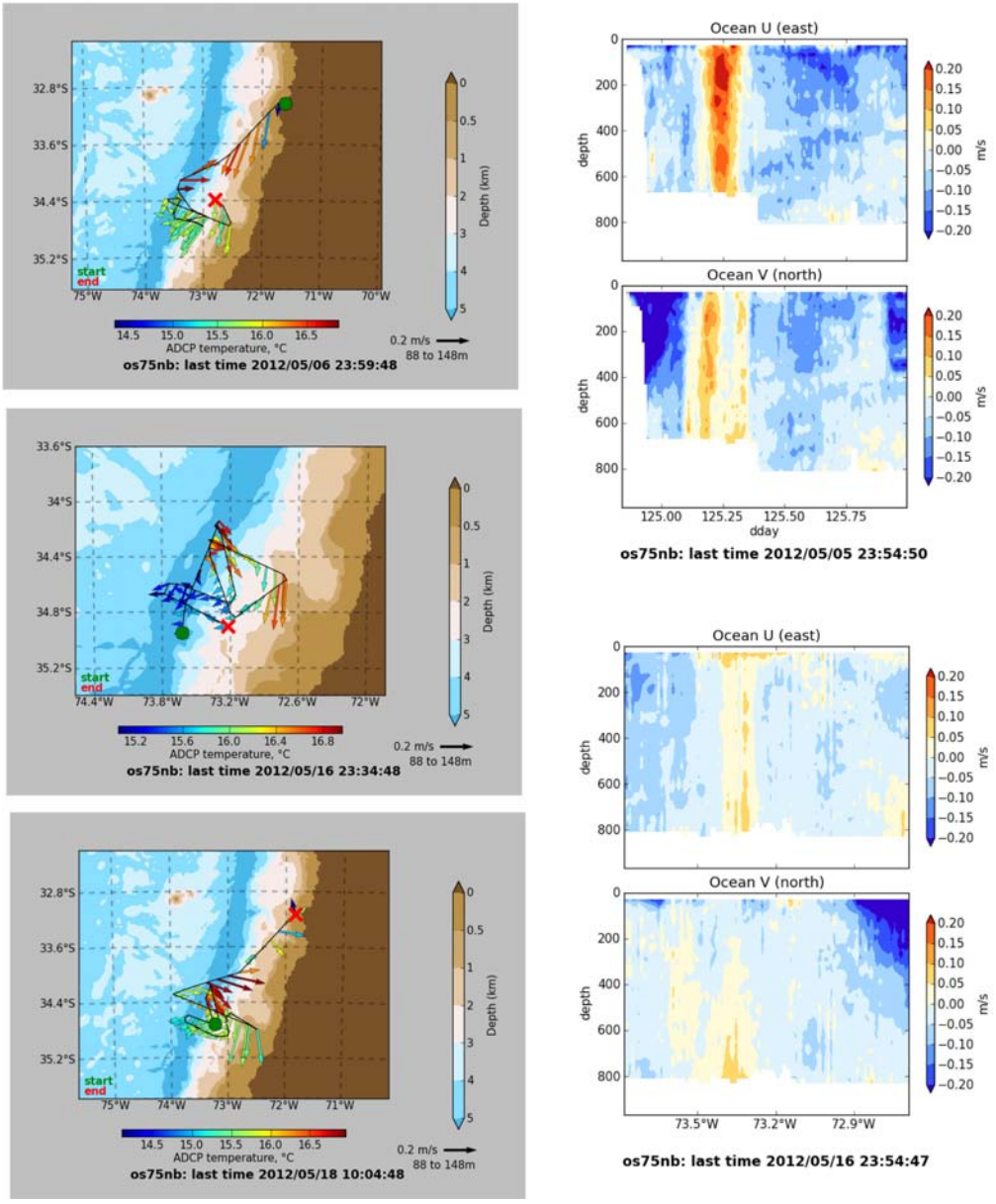

Figure 13. Examples of data plots from the ADCP image archive created during MV1206.

3.5 kHz sub-bottom profiler data:

Knudsen 3260 3.5 kHz subbottom profiling data were acquired during the entire cruise. The ping interval was synchronized with the EM122, resulting in a ping repetition interval that was not optimal for subbottom profiling. Data were recorded in both segy and Knudsen proprietary keb format. The keb files can be viewed with the free Knudsen viewer. Data can be downloaded from the Rolling Deck to Repository (R2R) web site (http://www.rvdata.us/catalog/MV1206).

MET data

Various types of standard under-way meterological data were acquired, including wind speed, surface water temperature. Data can be downloaded from the Rolling Deck to Repository (R2R) web site (http://www.rvdata.us/catalog/MV1206).

References:

Angermann, D., J. Klotz, and C. Reigber (1999), Space-geodetic estimation of the Nazca-South America Euler vector, *Earth Planet. Sci. Lett.*, (171), 3, 329-334.

Bangs, N.L., and S. C. Cande (1997), Episodic development of a convergent margin inferred from structures and processes along the southern Chile margin, *Tectonics*, *16(3)*, 489–503.

Bourgois, J., et al (2000), Glacial-interglacial trench supply variation, spreading-ridge subduction, and feedback controls on the Andean margin development at the Chile triple junction area (45°–48°S), *J. Geophys. Res.*, 105(B4), 8355–8386.

Contardo, X., J. Cembrano, A. Jensen, and J. Díaz- Naveas (2008), Tectono-sedimentary evolution of marine slope basins in the Chilean forearc (33°30′–36°50′S): Insights into their link with the subduction process, *Tectonophysics*, 459(1–4), 206–218.

Contreras-Reyes, E., E. R. Flueh, and I. Grevemeyer (2010), Tectonic control on sediment accretion and subduction off south central Chile: Implications for coseismic rupture processes of the 1960 and 2010 megathrust earthquakes, *Tectonics*, 29, doi:10.1029/2010TC002734.

Contreras-Reyes, E., and A. Osses (2010), Lithospheric flexure modeling seaward of the Chile trench: Implications for oceanic plate weakening in the Trench Outer Rise region, *Geophys. J. Int.*, 182(1), 97–112, doi:10.1111/j.1365-246X.2010.04629.

Davis, E. E., and H. W. Villinger (2006), Transient formation fluid pressures and temperatures in the Costa Rica forearc prism and subducting oceanic basement: CORK monitoring at ODP Sites 1253 and 1255, *Earth Planet. Sci. Lett.*, *245*, 232-244.

Davis, E. E., K. Wang, R. E. Thomson, K. Becker, and J. F. Cassidy (2001), An episode of seafloor spreading and associated plate deformation inferred from crustal fluid pressure transients, *J. Geophys. Res.*, *106*(B10), 21,953-921,963.

Davis, E. E., K. Becker, K. Wang, K. Obara, Y. Ito, and M. Kinoshita (2006), A discrete episode of seismic and aseismic deformation of the Nankai trough subduction zone accretionary prism and incoming Philippine Sea Plate, *Earth Planet. Sci. Lett.*, *242*, 73-84.

DeMets, C., R. G. Gordon, D. F. Argus, and S. Stein (1994), Effect of recent revisions to the geomagnetic reversal time scale on estimates of current plate motions, *Geophys. Res. Lett.*, 21(20), 2191–2194, doi:10.1029/94GL02118.

Flueh, E. R., and J. Bialas (2008) , SFB 574 (James Cook Cruise JC23-A&B: Chile-Margin-Survey), IFM-GEOMAR Repport 20, Geomar, Kiel, Germany.

Gonzalez, E. (1989), Hydrocarbon resources in the coastal zone of Chile, in Geology of the Andes and Its Relation to Hydrocarbon and Mineral Resources, edited by G. Ericksen et al., pp. 383–404, Circum-Pac. Counc. for Energy and Miner. Resour., Houston, Texas.

Kopf, A., B. Clennell, and K. M. Brown (2005), Physical properties of muds extruded from mud volcanoes: Implications for episodicity of eruptions and relationship to seismogenesis, in *Mud Volcanoes, geodynamics and seismicity*, edited by G. Martinelli and B. Panahi, pp. 263-283, NATO Science Series IV: Dordrecht (Springer).

Kukowski, N., and O. Oncken (2006), Subduction erosion: The “normal” mode of forearc material transfer along the Chilean margin?, in Frontiers in Earth Sciences, vol. 3, The Andes: Active Subduction Orogeny, edited by O. Oncken et al., pp. 217–236, Springer, Berlin

Labonte, A., K. Brown, and Y. Fialko (2009), Hydrologic detection and finite element modeling of a slow slip event in the Costa Rica prism toe, *J. Geophys. Res.*, *114*, 1-13.

Lange, D., et al (2012) , Aftershock seismicity of the 27 February 2010 Mw 8.8 Maule earthquake rupture zone, *Earth. Planet. Sci. Lett*, 317-318, 413-425, doi:10.1016/j.epsl.2011.11.034

Lorito, S., et al., (2011) . Limited overlap between the seismic gap and coseismic slip of the great 2010 Chile earthquake. *Nature Geoscience*, 1752-0908. doi:10.1038/ngeo1073.

Melnick, D and H. Echtler (2006), Inversion of forearc basins in south-central Chile caused by rapid glacial age trench fill, *Geology,* **34** (9), 709–712.

Moscoso, E., et al. (2011), Revealing the deep structure and rupture plane of the 2010 Maule, Chile earthquake (Mw=8.8) using wide angle seismic data, *Earth Plan. and Sci. Lett*., 307, 147-155., doi:10.1016/j.epsl.2011.04.025.

Rietbrock, A., I. Ryder, G. Hayes, C. Haberland, D. Comte, S. Roecker, and H. Lyon-Caen (2012), Aftershock seismicity of the 2010 Maule Mw=8.8, Chile, earthquake: Correlation between co-seismic slip models and aftershock distribution?, *Geophys. Res. Lett.*, 39, L08310, doi:10.1029/2012GL051308.

Roeloffs, E. A. (1996), Poroelastic techniques in the study of earthquake-related hydrologic phenomena, *Advances in Geophysics*, *37*, 135-195.

Scherwath, M., et al., (2009), Deep lithospheric structures along the southern central Chile Margin from wide-angle P-wave modelling, *Geophys. J. Int*., 179, 579–600, doi: 10.1111/j.1365-246X.2009.04298.x

Spinelli, G. A., E. R. Giambalvo, and A. T. Fisher (2004), Sediment permeability, distribution, and influence on fluxes in oceanic basement, in *Hydrogeology of the Oceanic Lithosphere*, edited by E. E. Davis and H. Elderfield, Cambridge University Press.

Thornburg, T.M., Kulm, D., Hussong, (1990), Submarine-fan development in the southern Chile trench: a dynamic interplay of tectonics and sedimentation, *Geol. Soc. Am. Bull,* 1658-1680.

Tryon, M. D. (2009), Monitoring aseismic tectonic processes via hydrologic responses: An analysis of log-periodic fluid flow events at the Costa Rica outer rise, *Geology*, *37*(2), 163-166.

Tryon, M. D., K. M. Brown, L. M. Dorman, and A. Sauter (2001), A new benthic aqueous flux meter for very low to moderate discharge rates, *Deep-Sea Res. I*, *48*(9), 2121-2146.

Voelker D., F. Scholz, and J. Geersen (2011), Analysis of submarine landsliding in the rupture area of the 27 February 2010 Maule earthquake, Central Chile, *Marine Geology*, 288, 79-89, doi:10.1016/j.margeo.2011.08.003.

von Huene, R., et al. (1997) , Tectonic control of the subducting Juan Fernandez Ridge on the Andean margin near Valparaiso, Chile, *Tectonics*, 16, 474-488.

Appendix 1:

Article about the cruise in a local newspaper prior to our departure from Valparaiso.

De Valparaíso zarpó crucero que estudiará placas sísmicas

GEOFÍSICA. *Expertos chilenos, en compañía de norteamericanos, realizarán por dos semanas un estudio que busca respuestas del continente tras terremoto.*

Desde Valparaíso zarpó un grupo de geofísicos de la Facultad de Ciencias Físicas y Matemáticas de la Universidad de Chile y de la Oregon State University, de Estados Unidos, acompañados por expertos del Scripps Institution of Oceanography, con el objetivo de investigar la zona de ruptura marina que dejó el terremoto producido en el país el 27 de febrero de 2010.

Para llevar a cabo esta larga investigación, que podría tardar hasta cinco años en entregar la totalidad de los resultados, los embarcados hasta Constitución (Región del Maule) depositarán entre 4 mil a 5 mil metros de profundidad, un total de 10 sismómetros en varios puntos. Un año después, los aparatos serán retirados para su estudio.

MIGUEL CAMPOS

DIEZ SISMÓMETROS INSTALARÁN FRENTE A LAS COSTAS DE CONSTITUCIÓN PARA LLEVAR A CABO EL ESTUDIO.

ESTUDIO

El buque Melville emprendió su viaje durante la tarde de ayer hasta la zona donde la placa de Nazca se subducta bajo la Sudamericana, con el objetivo de recorrer y estudiar durante dos semanas las deformaciones dejadas por el sismo de 8.8 grados Richter.

"Queremos estudiar la respuesta del continente en deformación producido por el deslizamiento del terremoto, es decir, cómo se forma y cómo se transmiten los esfuerzos hacia la parte más externa. En este lugar de la región no corresponde a roca dura, sino que son sedimentos que se llama prisma de acreción, entonces su deformación es muy distinta al contacto de roca dura oceánica con respecto a roca dura continental", informó el geofísico, Eduardo Contreras.

El estudio de la ubicación del límite entre la corteza continental con el prisma de acreción es fundamental para la estimación de la magnitud de los tsunamis y terremotos producidos al interior del mar, ya que el contacto entre ambas zonas controla la ubicación del límite superior de la zona sismogénica.

Sumario a Jumbo por ratones se entregará la próxima semana

SANIDAD. *Seremi de Salud confirm que "se encontraron deficiencias"*

Entre lunes o martes de la próxima semana finalizará el sumario realizado por la Seremi de Salud al supermercado Jumbo de Valparaíso, el que espera arrojar importantes resultados sobre la posible presencia de una plaga de ratones al interior de este establecimiento comercial.

La denuncia ante la Secretaría Ministerial fue hecha por el Sindicato de Trabajadores del local, quienes declararon que desde el año pasado se conoce la presencia de roedores, los que -según indican- no son ejemplares pequeños.

Pese a esta situación dada a conocer por funcionarios del mismo supermercado, el seremi de Salud (s), Juan Luis Solari, explicó que "no puedo dar mayores informaciones acerca del sumario que se está haciendo hasta que no se le notifique a la empresa. Una vez que se realice esto, se pueden hacer público los detalles. Por el momento sólo podemos decir que efectivamente se encontraron deficiencias".

Además, la autoridad (s) sanitaria agregó que "esto de los

DENUNCIAS SON DEL AÑ

ratones también s
otros casos donde h
contrado feca de pa
hasta palomas mism
rior de bodas de algu
tos comerciales, e
mente donde están l
tos o bien, donde s
nan estos mismos".

Sandra Báez, tes
síndicato regional d
dores de Jumbo, con
la intención de ellos
rrar el local, puesto q
ir en desmedro de l
chos casos- única fu
ral de la familia.

Appendix 2: Specifications of the OBSs deployed on the central Chile margin.

LDEO Standard Ocean-Bottom Seismometer

Ocean-Bottom Seismology Laboratory
Lamont-Doherty Earth Observatory
Columbia University | Earth Institute

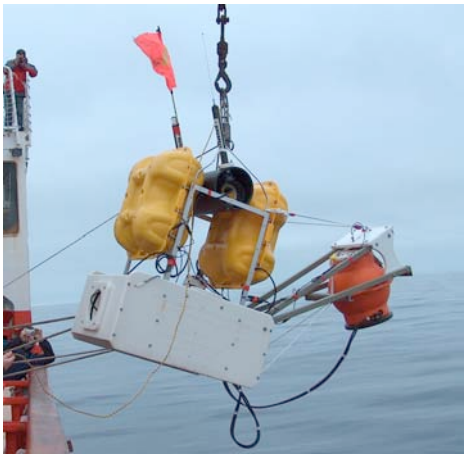

The LDEO standard seismometer design has been in use for nearly 10 years. The LDEO OBS lab has built and operates 25 standard OBSs as part of the NSF OBS Instrumentation Pool. The seismometer sensor is an L4C 1 Hz geophone, with a low-noise amplifier, giving useful response down to 100 s, and a differential pressure gauge. This instrument has been used in both year-long passive-source and shorter-term active-source experiments. The design includes dual redundancy with two transponders and two dropweights.

Variants and add-ons

Trawl-resistant OBS
Moored DPG/hydrophone
Ocean-bottom magnetometer
Diffuse flowmeter
Trillium Compact sensor
Absolute pressure gauge
Hydrophone

Specifications

Max. Depth	5000 m
Max. Duration	400 days @ 125 sps
Channels	4, 24-bit recording
Sensors	L4C 3-component geophones; differential pressure gauge
Response	100 s - 60 Hz (seismometer) 0-20 Hz (DPG)
Leveling system	Active 360°,motor-driven
Weight	750 lb in air
Footprint	3'X4'
Flotation	9X12" glass spheres
Sampling	40-100-125 sps
Release	Dual dropweights
Acoustics	Two ORE 12 kHz transponders
Power	Lithium battery pack, +/- 7.5 V
Oscillator	Seascan 10 MHz clock
Sensor housing	17" glass sphere
Burnwires	LDEO design
Recovery aids	Radio, strobe, flag
Recording	2 X 32 Gb CompactFlash cards
Dropweights	Two steel weights (75 lb in air)
Datalogger	LDEO ultra-low power OBS datalogger (300 mW @ 125 sps)

Deployment History

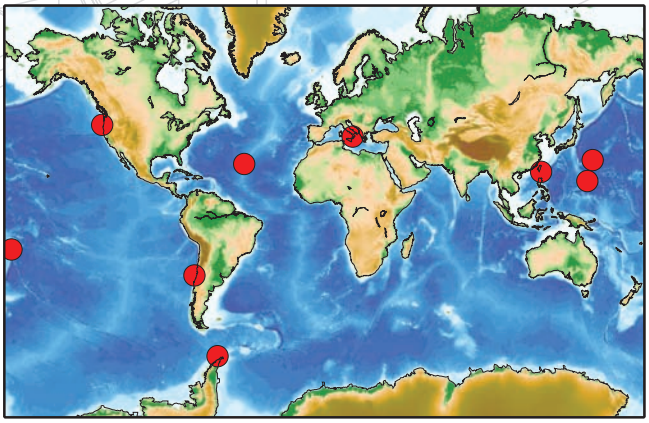

LDEO 2011 Model OBS

Ocean-Bottom Seismology Laboratory
Lamont-Doherty Earth Observatory
COLUMBIA UNIVERSITY | EARTH INSTITUTE

The LDEO 2011 seismometer design is a recent update of the standard LDEO design. Each OBS is equipped with a Trillium Compact seismometer, a Paroscientific absolute pressure gauge, and a hydrophone. The LDEO OBS lab has built 15 2011 OBSs: 5 for use in the standard OBSIP fleet and 10 for use in the Cascadia Initiative. The design includes dual redundancy with two transponders and two dropweights.

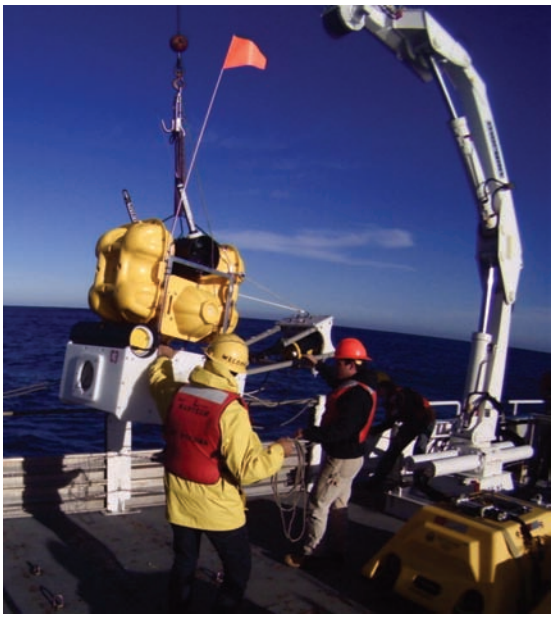

Specifications

Max. Depth	5000 m
Duration	400 days
Channels	6, 24-bit recording
Sensors	Trillium Compact seismometer absolute pressure gauge (APG) hydrophone
Response	120 s - 60 Hz (seismometer)
Leveling system	Active 360°,motor-driven
Weight	850 lb in air
Footprint	3'X4'
Flotation	11X12" glass spheres
Sampling	40, 100, or 125 sps
Release	Dual dropweights
Acoustics	Two ORE 12 kHz transponders
Power	Lithium battery pack, +/- 7.5 V
Oscillator	Seascan 10 MHz clock
Sensor housing	8" diameter Al tube
Burnwires	LDEO design
Recovery aids	Radio, strobe, flag
Recording	2 X 32 Gb CF cards (seismo) 1 X 16 Gb SD card (APG)
Dropweights	Two steel weights (100 lb in air)
Datalogger	LDEO OBS datalogger LDEO APG datalogger

Deployment History

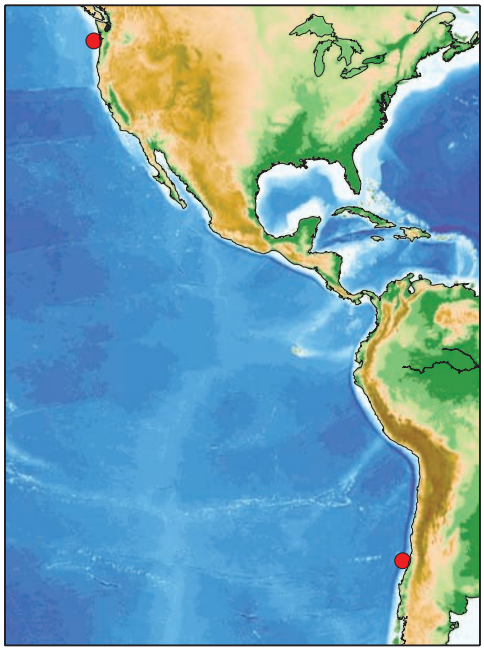

Appendix 3: Surveys to relocate OBSs on the seafloor.

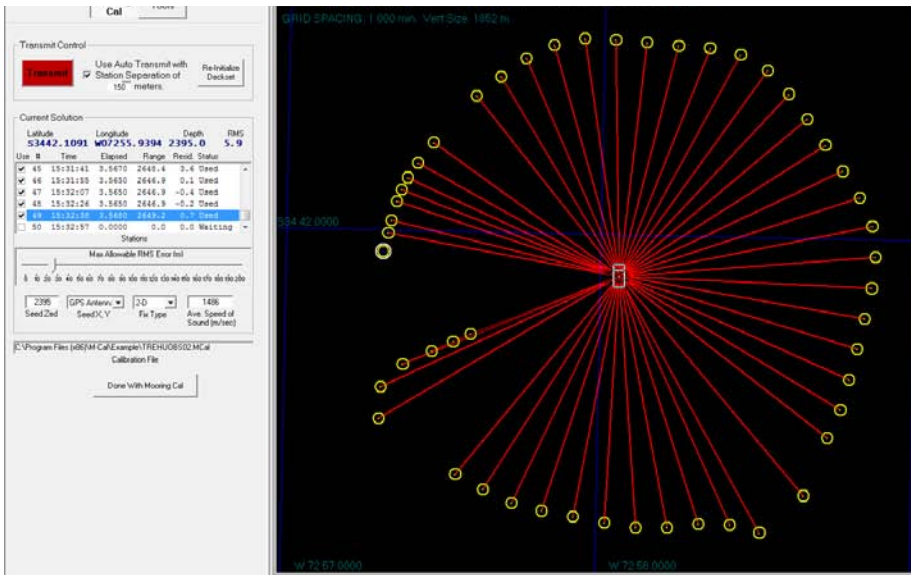

Site Name: OBS01ALT
Latitude: S 34° 42.1091’
Longitude: W 072° 55.9394’
Latitude Longitude in decimal degrees: -34.70181833 -72.93232333
Depth: 2395m RMS: 5.9m

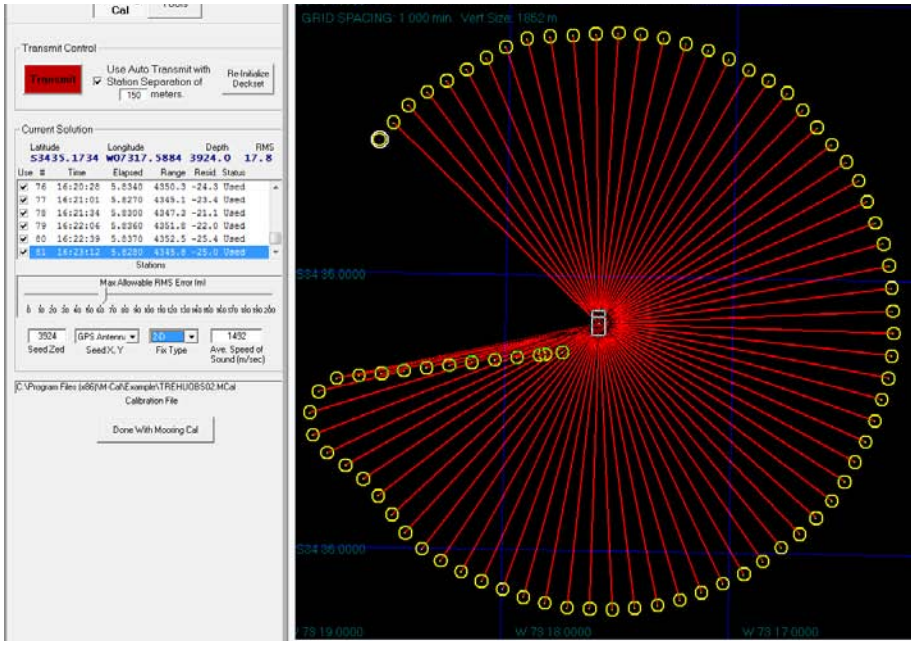

Site Name: OBS02
Latitude: S 34° 35.1734’
Longitude: W 073° 17.5884’
Latitude / Longitude in decimal degrees: -34.58622333 -73.29314
Depth: 3924m RMS: 17.8m

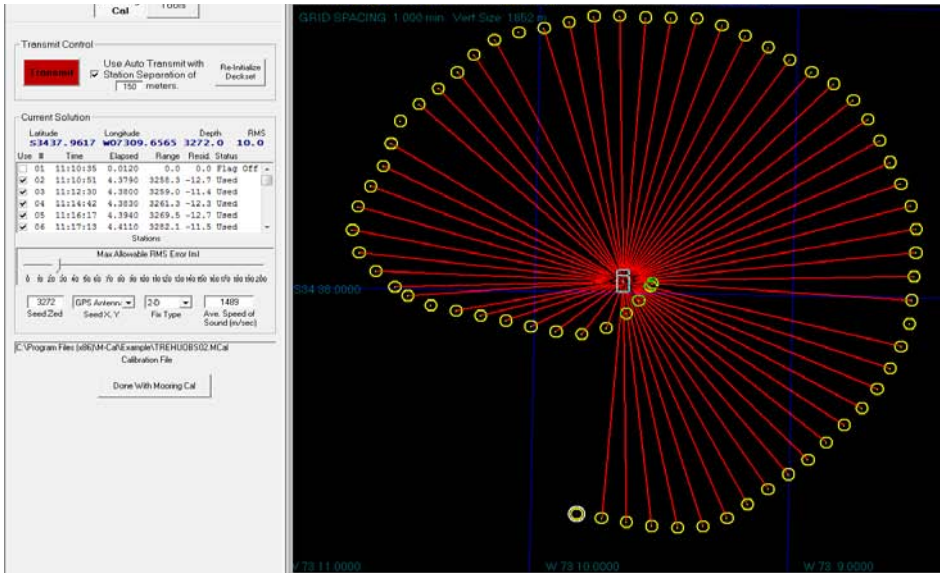

Site Name: OBS03
Latitude: S 34° 37.9617’
Longitude: W 073° 09.6565’

Latitude / Longitude in decimal degrees: -34.632695 -73.16094167
Depth: 3272m RMS: 10m

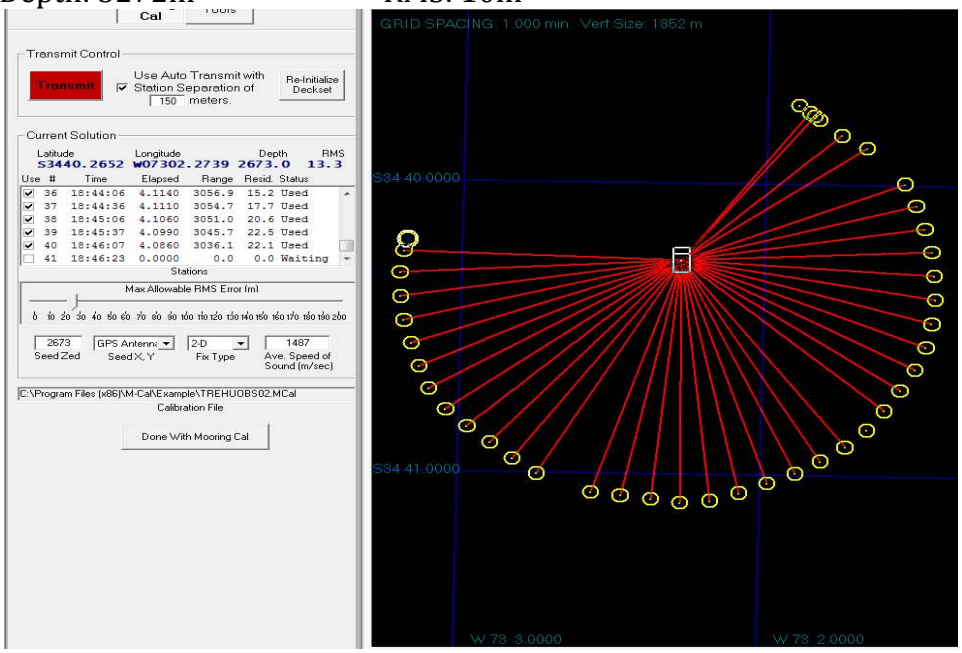

Site Name: OBS04
Latitude: S 34° 40.2652’
Longitude: W 073° 02.2739’
Latitude / Longitude in decimal degrees: -34.67108667 -73.03789833
Depth: 2673m RMS: 13.3m

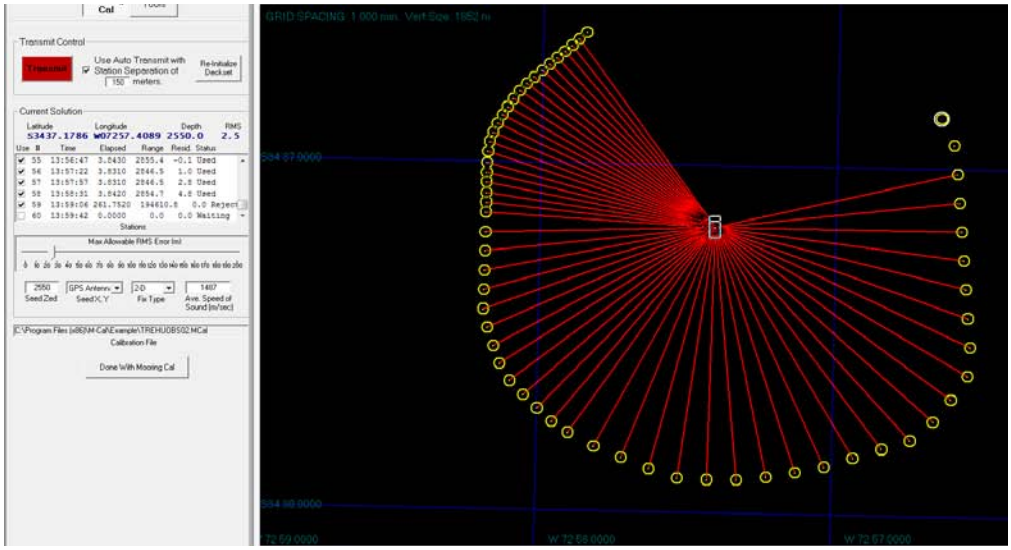

Site Name: OBS05ALT
Latitude: S 34° 37.1786’
Longitude: W 072° 57.4089’
Latitude / Longitude in decimal degrees: -34.61964333 -72.956815
Depth: 2550m RMS: 2.5m

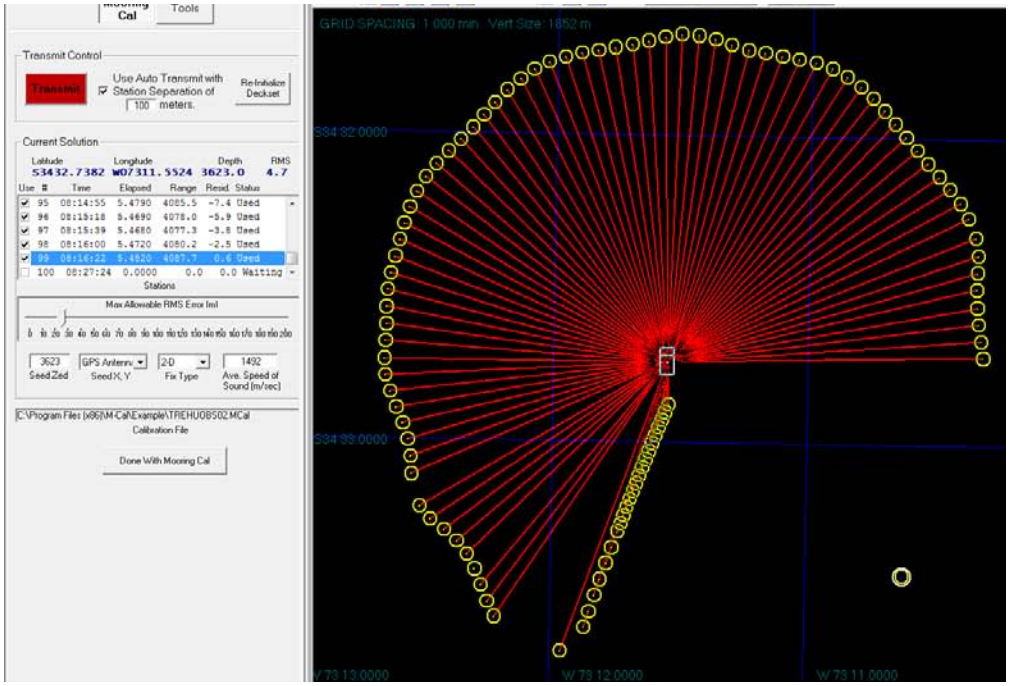

Site Name: OBS06
Latitude: S 34° 32.7382’
Longitude: W 073° 11.5524’
Latitude / Longitude in decimal degrees: -34.54563667 -73.19254
Depth: 3623m RMS: 4.7m

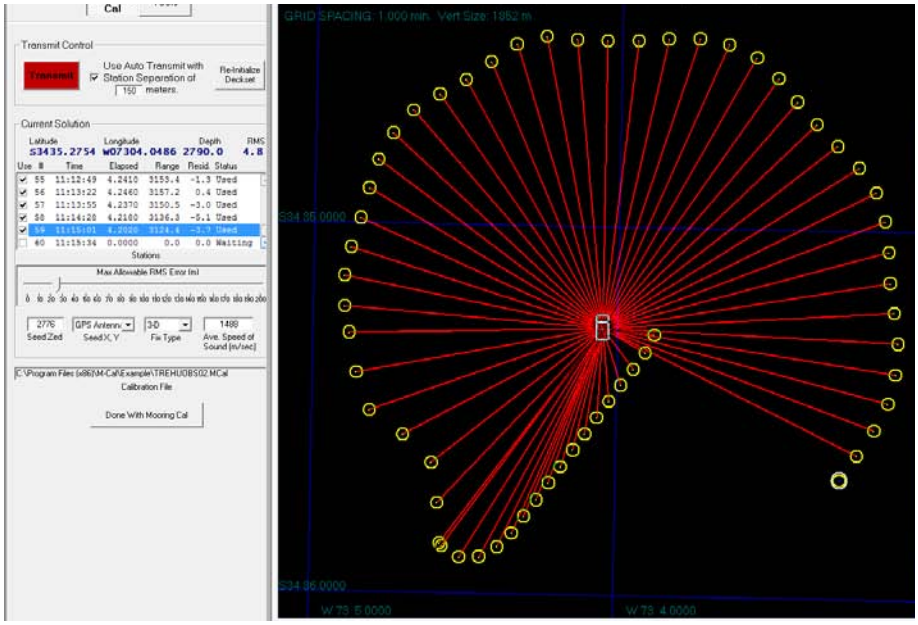

Site Name: OBS07
Latitude: S 34° 35.2754’
Longitude: W 073° 04.0486’
Latitude / Longitude in decimal degrees: -34.58792333 -73.06747667
Depth: 2790m RMS: 4.8m

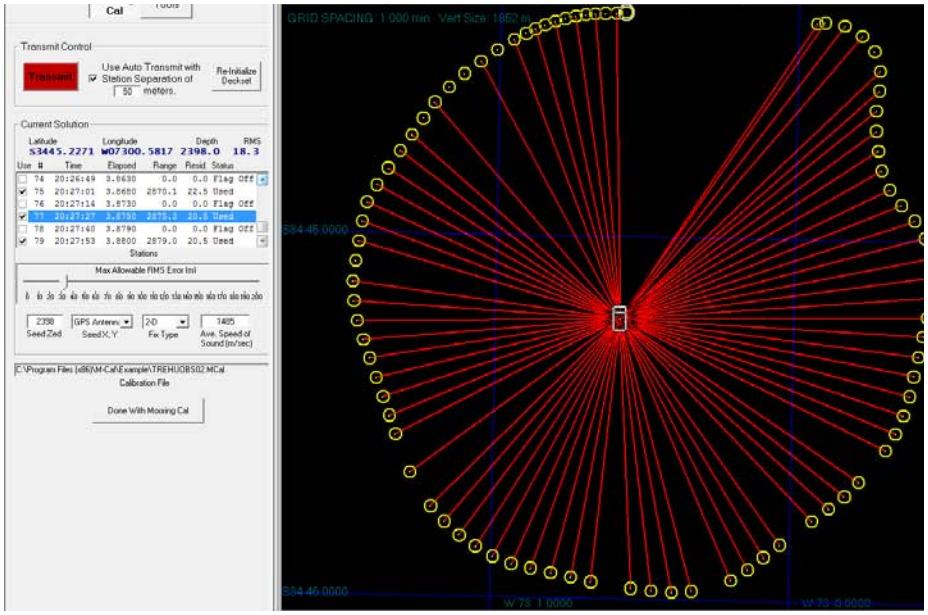

Site Name: OBS08
Latitude: S 34° 45.2271’
Longitude: W 073° 00.5817’
Latitude / Longitude in decimal degrees: -34.753785 -73.009695
Depth: 2398m RMS: 18.3m

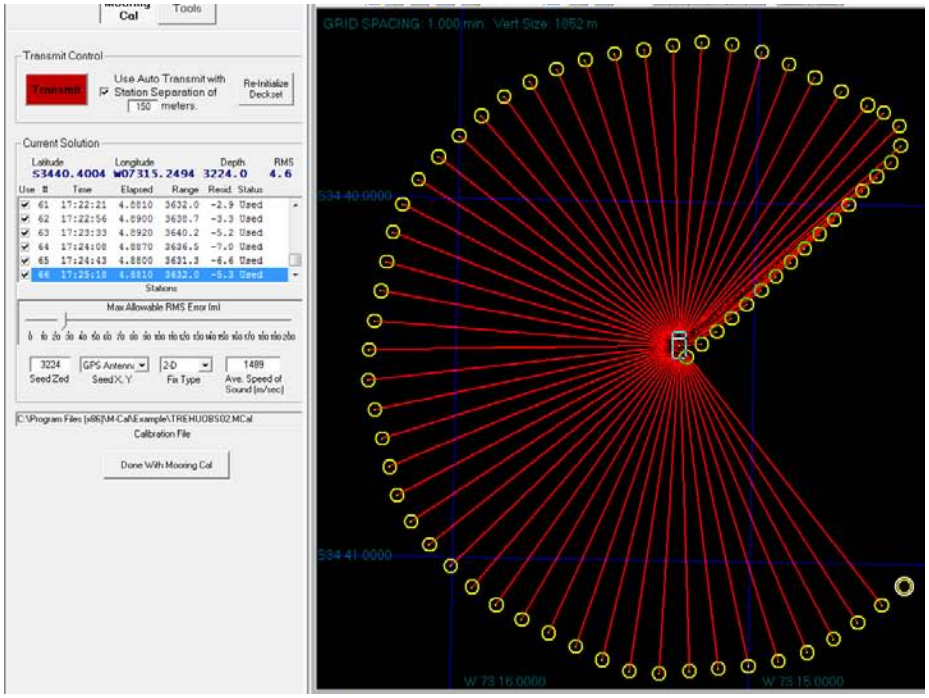

Site Name: OBS09
Latitude: S 34° 40.4004’
Longitude: W 073° 15.2494’
Latitude / Longitude in decimal degrees: -34.67334 -73.25415667
Depth: 3224m RMS: 4.6m

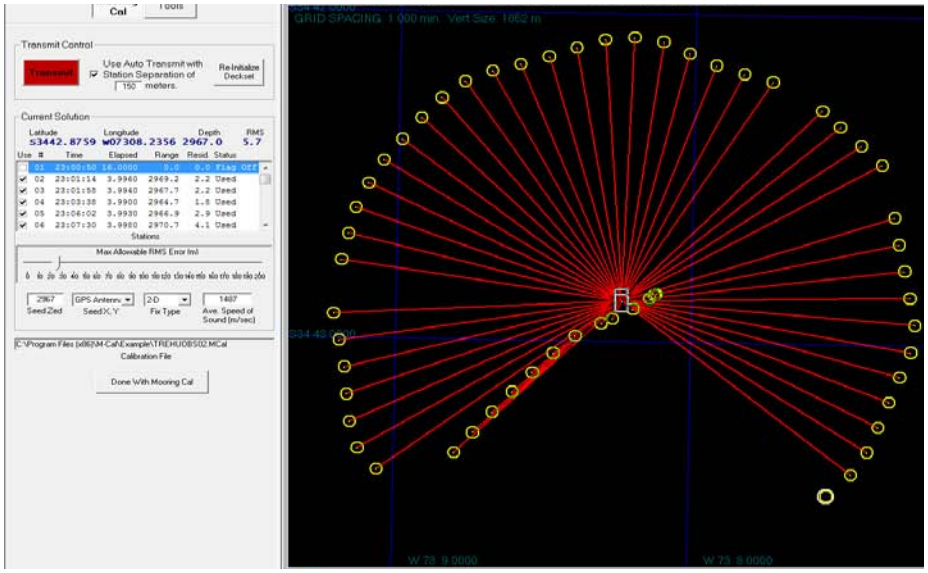

Site Name: OBS10
Latitude: S 34° 42.8759’
Longitude: W 073° 08.2356’
Latitude / Longitude in decimal degrees: - 34.71459833 -73.13726
Depth: 2967m RMS: 5.7m

Appendix 4: Abstracts and poster presented at the Fall 2012 meeting of the American Geophysical Union.

CONTROL ID: 1503294
TITLE: Structure of the accretionary prism up-dip of the M8.8 Maule earthquake rupture
AUTHORS (FIRST NAME, LAST NAME): Anne M Trehu[1], Michael D Tryon[2], Emilio E Vera[3], Eduardo Contreras-Reyes[3], Lee Ellett[2], Mark C Williams[1], Andrei Maksymowicz[3]
INSTITUTIONS (ALL): 1. College of Earth Ocean and Atmospheric Sciences, Oregon State University, Corvallis, OR, United States.
2. Scripps Institution of Oceanography, La Jolla, CA, United States.
3. Universidad de Chile, Santiago, Chile.
ABSTRACT BODY: In May 2012, we deployed 10 ocean bottom seismometers with integrated flow meters to record the post-seismic response of the accretionary prism up-dip from the patch of greatest slip during the M8.8 Maule earthquake on Feb. 27, 2010. Multiple lines of evidence indicate that significant slip and seafloor motion did not extend to the trench during this event, unlike during the 2011 Tohoku earthquake. As a result, the tsunami generated by this event, while locally devastating, was not as large or damaging as it might have been. Although constraints on the dynamic response of the prism to this event will not be available until the OBSs are recovered in spring 2013, we also had the opportunity to collect 1500 km of high resolution seismic reflection data, which help to define deformation patterns from the seaward to the landward boundary of the active prism. The reflection data show dramatic rapid variations along strike in the ratio of sediment subduction to sediment accretion at the trench and the presence of a large slump block in the trench that pre-dates the 2010 earthquake. We are examining the impact of buried topography and variations in trench sedimentation on the deformation front. At the eastern boundary of the accretionary prism, the new data indicate a complex boundary transpressional boundary overlying the seaward boundary of the continental backstop, and the seafloor morphology is shaped by interaction between tectonics and canyon cutting by the offshore extension of major rivers. The results presented here reflect the accumulated effect of multiple past megathrust earthquakes and will help to put the anticipated OBS results in a broader context.

KEYWORDS: [3060] MARINE GEOLOGY AND GEOPHYSICS / Subduction zone processes, [7240] SEISMOLOGY / Subduction zones.
(No Image Selected)
(No Table Selected)

Additional Details
Previously Presented Material: 0%

Contact Details
CONTACT (NAME ONLY): Anne Trehu
CONTACT (E-MAIL ONLY): trehu@coas.oregonstate.edu
TITLE OF TEAM:

Structure of the Accretionary Prism Updip of the M8.8 Maule Earthquake Rupture

Anne Tréhu[1], Mike Tryon[2], Emilio Vera[3], Eduardo Contreras-Reyes[3], Lee Ellett[2], Mark Williams[1], Andrei Maksymowicz[3]

1. College of Earth Ocean & Atmospheric Sciences, Oregon State University; 2. Scripps Institution of Oceanography; 3. Universidad de Chile Santiago

Background:

Several lines of evidence indicate that rupture during the 2010 M8.8 Maule earthquake offshore central Chile did not extend to the trench, in contrast to the 2011 Tohoku earthquake. As a result, the tsunami generated by this event, while locally devastating, was not as large or damaging as it might have been.

In May 2012, we deployed 10 ocean bottom seismometers with integrated flow meters to record the post-seismic response of the accretionary prism updip from the patch of greatest slip. Although constraints on the dynamic response of the prism to this event will not be available until the OBSs are recovered in spring 2013, we also collected 1500 km of high-resolution seismic-reflection data, which help to define deformation history of the prism. In this poster we present some preliminary results from the seismic reflection data.

Ultimately our objective is to understand how slip on the megathrust is accommodated within the accretionary complex and whether there are geologic characteristics of the margin that can be used to estimate tsunamigenic potential. Although post-seismic and inter-seismic slip down-dip of the zone that ruptures in great megathrust earthquakes has gotten a lot of attention in past years, the post-seismic slip up-dip of rupture is virtually unknown.

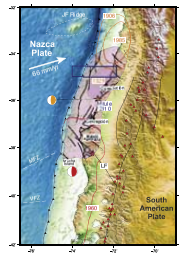

Map of the central Chile margin showing the tectonic setting and the rupture planes of the 2010 and previous historic earthquakes (from Moscoso et al., 2011).

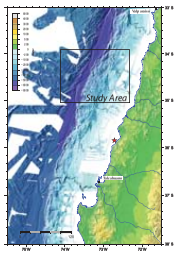

Bathymetric map of the central Chile continental margin . Data from GEOMAR, acquired during several surveys in 2008.

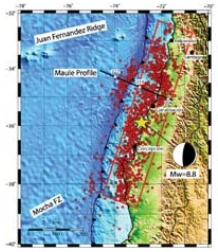

Aftershocks of the 2010 earthquake from Moscoso et al., EPSL, 2012. Note intense aftershock activity in the subducting plate at the latitude of the study area and the relative lack of aftershocks in the accretionary prism.

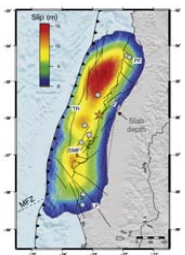

Slip model from Moreno et al. (EPSL, 2012). While slip models depend somewhat on the data used, all models show the greatest slip near 35 S.

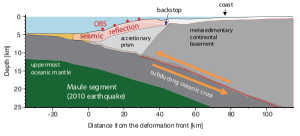

Cross-section through the Chile margin at the latitude of this study based on OBS/onshore reflection analysis (adapted from Contreras-Reyes, Tectonics, 2010).

New data:

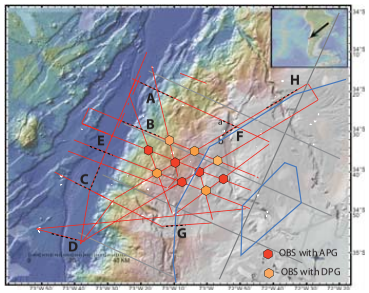

Gray lines show the location of seismic reflection data acquired in 2002 as part of the FONDEF project. Light blue lines shown the 10 and 15m slip contours from Lorito et al. (Nature Geoscience, 2011). Red lines show new data acquired for this project. Dashed segments are shown in this poster, with letters keyes to the data images. Yellow line is a bathymetric profile that was acquired over a track previously mapped in 2008 and 2010.

The seismic source was 2 GI guns shot simultaneously at 25 m interval. The shots were initially recorded on a 48-channel, 600-m long streamer. However, for most of the data, only 40 channels were available as streamer sections were damaged by sharks. Data were processed through f-k migration on board.

In addition, gravity and EM300 swath bathymetry were collected along all track lines. Magnetic anomaly data were collected along some tracks. A total of 26 XBTs were acquired during the cruise to provide groundtruth for possible "seismic oceanography."

Landward edge of the accretionary complex:

Crossings of a topographic channel (G) and ridge (H) over the landward edge of the accretionary prism show evidence for recent faulting and folding. The new data will provide a better understanding of the interaction between tectonics and erosion along this boundary, which coincides with the seaward edge of the high-slip patch during the 2010 earthquake.

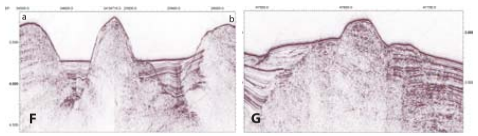

Cruise MV1206 Science Party

Oregon State University
Anne Trehu, chief scientist
Chris Kenyon, student
Yi Lou, visiting student
Mark Williams, student

Universidad de Chile Santiago
Emilio Vera Sommer, professor
Eduardo Contreras Reyes, professor
Emilio Bravo, student
Natalia Cornejo, student
Felipe Gonzalez, student
Andrei Maksymowicz, student

Chilean Observer
Patricio Opaza Arriagada

Scripps Institution of Oceanography
Mike Tryon, co-chief scientist
Lee Ellett, seismic technician
Jon Meyer, computer technician
Keith Shadle, technician
Jay Turnbull, seismic technician

Lamont Doherty Earth Observatory
David Gassier, OBS engineer
Ted Koczynski, OBS engineer
Vincent Oletu, OBS technician
Drew Stolzman, OBS technician

Marine Mammal Observers
Chris Cutler
Patti Haase
Paula Olson

This work is funded by the National Science Foundation. Seismic data were processed using SIOSEIS software and displayed using Kingdom Suite, donated by Seismic Micro-Technology to Oregon State University. Bathymetric data were processed using MBsystem and displayed with GMT and GeoMapApp.

Deformation front:

The deformation front was crossed 12 times during the seismic survey. In spite of the small source volume, the top of the subducting crust can be traced up to 10 km landward of the deformation front, where a wide variety of deformation styles is observed. On Line A, essentially all the sediment is currently being accreted, whereas on Line B, located approximately 10 k to the south, nearly all the sediment is being underthrust, resulting in a well-defined subduction channel. A reflection that could be the roof of an earlier subduction channel is observed up slope. Other crossings are intermediate between A and B.

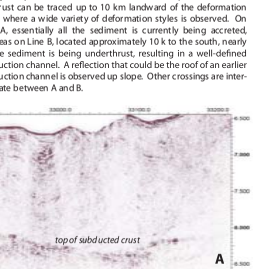

Some questions to address concerning sediment accretion/subduction:
- Is accretion v.s. subduction controlled by basement topography and/or the composition of near-surface trench sediment?
- Does sediment subduction lead to over-steepened slopes and more slope instability?

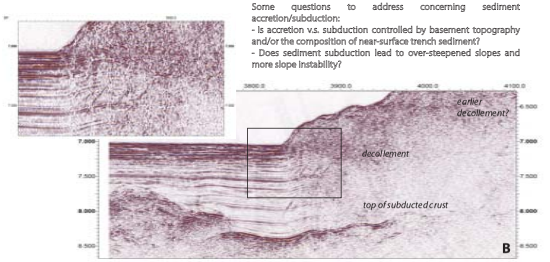

Trench:

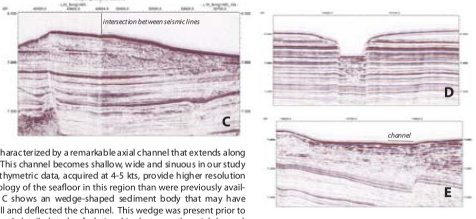

The Chile trench is characterized by a remarkable axial channel that extends along much of its length. This channel becomes shallow, wide and sinuous in our study region. The new bathymetric data, acquired at 4-5 kts, provide higher resolution data on the morphology of the seafloor in this region than were previously available. Seismic line C shows an wedge-shaped sediment body that may have loaded the trench fill and deflected the channel. This wedge was present prior to the 2010 earthquake. A detailed study of relationships between the axial channel, subsurface structure and seafloor morphology is ongoing.

Canyons and slope stability:

The Mataquito river canyon shows spectacular slump scars along its walls. The seismic data reveal a sequence of slumps and redirections of this submarine river that will provide insights into canyon processes. Section H also shows a Bottom Simulating Reflection (BSR) indicative of the presence of gas hydrates. A low-amplitude BSR is observed throughout much of the region covered by this survey. Anomalously bright or shallow BSRs, or other indicators of active venting, were not observed.